NGR-25-001-055

NUMERICAL SOLUTION OF THE NAVIER-STOKES EQUATIONS FOR HIGH REYNOLDS NUMBER INCOMPRESSIBLE TURBULENT FLOW

By

David S. Thompson

A Thesis
Submitted to the Faculty of
Mississippi State University
in Partial Fulfillment of the Requirements
for the Degree of Master of Science
in the Department of Aerospace Engineering

Mississippi State, Mississippi

May, 1980

NUMERICAL SOLUTION OF THE NAVIER-STOKES EQUATIONS FOR HIGH REYNOLDS NUMBER INCOMPRESSIBLE TURBULENT FLOW

By

David S. Thompson

A Thesis
Submitted to the Faculty of
Mississippi State University
in Partial Fulfillment of the Requirements
for the Degree of Master of Science
in the Department of Aerospace Engineering

Mississippi State, Mississippi

May, 1980

NUMERICAL SOLUTION OF THE NAVIER-STOKES EQUATIONS FOR HIGH REYNOLDS NUMBER INCOMPRESSIBLE TURBULENT FLOW

By

David S. Thompson

APPROVED:

Professor and Head of the Department of Aerospace Engineering	Director of Graduate Instruction, College of Engineering
Professor of Aerospace Engineering (Major Professor)	Dean of the College of Engineering
Dean of the Graduate School	

May, 1980

ACKNOWLEDGEMENTS

The author wishes to express his sincere gratitude to his major professor, Dr. Joe F. Thompson, for his direction and guidance in this Masters program. Thanks are also due Mr. Charles B. Cliett, Professor and Head of the Department of Aerospace Engineering, for his moral and financial support during this program. Thanks are also due the other faculty members and the graduate students of the Department of Aerospace Engineering.

Thanks are also due Frank Thames and Kitty Haigler of the NASA Langley Research Center for their assistance in the conversion of the computer code.

The author also wishes to thank Mrs. Nancie Upchurch for her excellent typing of the final manuscript, and Mr. Jim Henson for his preparation of the figures. In addition, the author would like to thank his fiancée for the moral support provided and the assistance given in the preparation of this manuscript.

Finally, the author would like to thank his parents for making his undergraduate education possible.

The partial support of NASA Grant NGR-25-001-055, is gratefully acknowledged.

D.S.T.

Mississippi State University

May 1980

ABSTRACT

David S. Thompson, Master of Science, 1980

Major: Aerospace Engineering, Department of Aerospace Engineering

Title of Thesis: Numerical Solution of the Navier-Stokes Equations for High Reynolds Number Incompressible Turbulent Flow

Directed by: Dr. Joe F. Thompson

Pages in Thesis: 58 Words in Abstract: 198

Abstract

The full Navier-Stokes equations for incompressible turbulent flow must be solved to accurately represent all flow phenomena which occur in a high Reynolds number incompressible flow. A two-layer algebraic eddy viscosity turbulence model is used to represent the Reynolds stress terms in the time-averaged incompressible Navier-Stokes equations in the primitive variable formulation. The development of the boundary-fitted coordinate systems has made the numerical solution of these equations feasible for arbitrarily shaped bodies.

The non-dimensional time-averaged Navier-Stokes equations, including the turbulence model, are represented by finite difference approximations in the transformed (ξ,η) plane. The resulting coupled system of nonlinear algebraic equations is solved using a point successive over-relaxation (SOR) iteration.

The test case considered in this study was an NACA 64A010 airfoil section at an angle of attack of two degrees and a Reynolds number of 2,000,000. Several boundary-fitted coordinate systems

were generated and used to evaluate various filters and various representations of the convective terms. Pressure distributions are presented which emphasize the difficulties associated with each technique.

The preliminary results of a solution are presented which encourage the continuation of the solution to obtain a steady state solution. The major results of the evaluation of the techniques are also summarized.

TABLE OF CONTENTS

LIST OF SYMBOLS

Symbol	
D	Continuity Equation
f	General Function of ξ, η, and t
i	As a Subscript, Position in Discrete Mesh System
j	As a Subscript, Position in Discrete Mesh System
J	Jacobian Determinant, Equation (A.8)
L	Characteristic Length (Chord)
n	As a Superscript, Time Level
$P(\xi,\eta)$	ξ-Line Attraction Function
p	Pressure
p_w	Pressure on the Wall (Body)
$Q(\xi,\eta)$	η-Line Attraction Function
Re	Reynolds Number Based on Chord Length
s	Iteration Counter
t	Time; as a Subscript, Partial Differentiation with Respect to Time
u	Velocity Component Parallel to x-Axis
U_∞	Freestream Velocity
v	Velocity Component Parallel to y-Axis
x	Physical Cartesian Coordinate; as a Subscript, Partial Differentiation with Respect to x
y	Physical Cartesian Coordinate; as a Subscript, Partial Differentiation with Respect to y
α	Coordinate Transformation Parameter, Equation (A.1)
β	Coordinate Transformation Parameter, Equation (A.2)

γ	Coordinate Transformation Parameter, Equation (A.3)
Γ_i	i^{th} Contour in Physical Plane
Γ_i^*	Contour in Transformed Plane Corresponding to Γ_i
ϵ	Ratio of μ_t to μ
η	Transformed Coordinate; as a Subscript, Partial Differentiation with Respect to η
θ	Switch for Shuman Filter
μ	Molecular Coefficient of Viscosity
μ_t	Eddy Viscosity Coefficient Obtained from Turbulence Model
ξ	Transformed Coordinate; as a Subscript, Partial Differentiation with Respect to ξ
ρ	Fluid Density
σ	Coordinate Transformation Parameter, Equation (A.6)
τ	Coordinate Transformation Parameter, Equation (A.7)
ϕ	Angle of Attack
ω	Constant Acceleration Parameter Used in Calculation of Optimum Acceleration Parameter for Chorin-Type Iteration for Wall Pressure
Ω	Optimum Acceleration Parameter for Chorin-Type Iteration for Wall Pressure, Equation (3.8b)
*	As a Superscript, Non-Dimensional Quantity (Γ_i^* is an Exception)
$'$	As a Superscript, Fluctuation Quantity
$\bar{}$	As a Superscript, Time-Averaged Quantity

LIST OF FIGURES

I. INTRODUCTION

The problem of accurately predicting the flowfield about an arbitrary configuration in a high Reynolds number incompressible flow has provided seemingly insurmountable problems to researchers in this area. The only way to represent fully all flow phenomena which occur at these conditions is to solve the full Navier-Stokes equations for incompressible turbulent flow. The primitive variable formulation must be used if multiple bodies or three-dimensional flow is to be considered.

Since the solution of the Navier-Stokes equations is essentially a very complex boundary value problem, the validity of the solution is dependent on the accuracy of the representation of the boundary values. If a conventional grid system is used for an arbitrary configuration, interpolation will be required at the boundaries. This may lead to poor application of the boundary conditions. In high Reynolds number flow, there are large gradients in regions near solid boundaries. These gradients are generally dominant in determining the character of the solution. The resolution of these gradients requires that a large number of closely spaced coordinate lines exist in the regions near solid boundaries. This would suggest using a fine mesh near these boundaries and a coarse mesh in the regions where the gradients are small with some type of transitional mesh in between.

A technique has been developed by Thompson, Thames, and Mastin [1] which will help to alleviate these problems. This technique numerically generates a discrete mesh system, called a boundary-fitted coordinate system, for arbitrary configurations. These mesh systems possess a constant coordinate line coincident with each physical

boundary so interpolation is eliminated at the boundaries. By modifying the governing equations, coordinate lines can be concentrated in any region of the field.

The two-dimensional Navier-Stokes equations for incompressible turbulent flow are represented by a finite difference approximation for the time-averaged incompressible Navier-Stokes equations and a slightly modified version of the algebraic turbulence model developed by Baldwin and Lomax [2]. The finite difference approximations must be augmented by the inclusion of terms relating the discrete mesh and the physical grid. This effectively removes the physical coordinate system from the problem at the expense of complicating the original set of equations. However, application of the boundary conditions is simplified since the boundary conditions are given on straight boundaries in the transformed plane. Since the finite difference approximations represent an elliptic system of nonlinear partial differential equations, an iterative technique must be used to obtain a solution. The technique used in this study was an accelerated Gauss-Seidel iteration, or successive over-relaxation (SOR).

These techniques have been used with some success for incompressible viscous flow by several researchers. Bearden [3] obtained results for laminar flow at a Reynolds number of 1,000,000 about a single element airfoil at zero angle of attack using the stream function-vorticity formulation of the Navier-Stokes equations. Reddy [4] also obtained results for the same flow conditions using the integro-differential formulation. Primitive variable formulations have been developed by Hodge [5] and Shanks [6]. Hodge [5] obtained results for laminar flow about a single element airfoil at zero angle of attack for a Reynolds

number of 41,400. Shanks [6] considered low Reynolds number flow about a submerged hydrofoil.

II. THE BOUNDARY-FITTED COORDINATE SYSTEM

Much research has been devoted to the development of the techniques necessary for numerically generating boundary-fitted coordinate systems. Since the mathematical development and numerical implementation of these techniques is given in great detail by Thompson, Thames, and Mastin [1], Hodge [5], Thompson [7], and Thames [8], only an overview will be presented here. In addition, a method used to contract coordinate lines near a body in the field is given in Appendix B.

Consider a two-dimensional doubly-connected region as shown in Figure 1. The general transformation is one which associates each point (x,y) in the physical plane with a corresponding point (ξ,η) in the transformed plane. Let $\eta = \eta_1$ on the body contour Γ_1 and $\eta = \eta_2$ on the outer boundary Γ_2. The contour Γ_1 in the physical plane maps to the contour Γ_1^* in the transformed plane. Similarly, the contour Γ_2 maps to the contour Γ_2^*. The contours Γ_3 and Γ_4 represent a "cut" to be made in the physical plane and constitute the reentrant segments, Γ_3^* and Γ_4^*, in the transformed plane. Let $\xi = \xi_1$ on Γ_4 and $\xi = \xi_2$ on Γ_3. ξ is allowed to vary monotonically from ξ_1 to ξ_2 on both the inner and outer boundaries, Γ_1 and Γ_2 respectively. The values of the physical coordinates on Γ_3 and Γ_4 are the same, but the function $\xi = \xi(x,y)$ is multivalued on Γ_3 and Γ_4 since $\xi_1 \neq \xi_2$.

Now ξ and η have been completely specified on all the boundaries of a closed field. It remains to define the values in the interior of the field in terms of these boundary values. This implies that elliptic partial differential equations can be used to generate the field points since the solution of an elliptic partial differential equation is

completely defined in the interior of a region by its values on the boundaries of that region. The elliptic system chosen must exhibit certain maximum principles which preclude the occurrence of extrema in the interior of the region. This will assure that a one-to-one correspondence exists between the physical and the transformed plane.

The generating system of equations used in this study is a slightly modified version of the elliptic systems given by References [1], [5], [7], and [8]. The elliptic system used to generate the boundary-fitted coordinate system is given by

$$\xi_{xx} + \xi_{yy} = -\frac{\alpha}{J^2} P(\xi,\eta) \tag{2.1a}$$

$$\eta_{xx} + \eta_{yy} = -\frac{\gamma}{J^2} Q(\xi,\eta), \tag{2.1b}$$

subject to the following Dirichlet boundary conditions

$$\begin{bmatrix} \xi \\ \\ \eta \end{bmatrix} = \begin{bmatrix} \xi_1(x,y) \\ \\ \eta_1 \end{bmatrix}, \quad [x,y] \epsilon \Gamma_1 \tag{2.2a}$$

$$\begin{bmatrix} \xi \\ \\ \eta \end{bmatrix} = \begin{bmatrix} \xi_2(x,y) \\ \\ \eta_2 \end{bmatrix}, \quad [x,y] \epsilon \Gamma_2 \tag{2.2b}$$

where $P(\xi,\eta)$ and $Q(\xi,\eta)$ are the attraction functions for the ξ and η lines respectively and α, γ and J are given, along with other quantities relating the physical and the transformed planes in Appendix A. Since it is desired that all numerical computations be performed in the

transformed plane, the independent and dependent variables must be interchanged. In the transformed plane, the generating system is given by

$$\alpha x_{\xi\xi} - 2\beta x_{\xi\eta} + \gamma x_{\eta\eta} = -(\alpha x_{\xi} P(\xi,\eta) + \gamma x_{\eta} Q(\xi,\eta)) \tag{2.3a}$$

$$\alpha y_{\xi\xi} - 2\beta y_{\xi\eta} + \gamma y_{\eta\eta} = -(\alpha y_{\xi} P(\xi,\eta) + \gamma y_{\eta} Q(\xi,\eta)) \tag{2.3b}$$

with the transformed boundary conditions

$$\begin{bmatrix} x \\ y \end{bmatrix} = \begin{bmatrix} f_1(\xi,\eta_1) \\ f_2(\xi,\eta_1) \end{bmatrix}, \quad [\xi,\eta_1] \in \Gamma_1^* \tag{2.4a}$$

$$\begin{bmatrix} x \\ y \end{bmatrix} = \begin{bmatrix} g_1(\xi,\eta_2) \\ g_2(\xi,\eta_2) \end{bmatrix}, \quad [\xi,\eta_2] \in \Gamma_2^* \tag{2.4b}$$

where the definition of β is given in Appendix A. The functions $f_1(\xi,\eta_1)$, $f_2(\xi,\eta_1)$, $g_1(\xi,\eta_2)$, and $g_2(\xi,\eta_2)$ are specified by the known shape of the contours Γ_1 and Γ_2 respectively, and the specified ξ distribution thereon.

Even though this system of quasi-linear partial differential equations, Equations (2.3a) and (2.3b), is more complicated than the original system, Equations (2.1a) and (2.1b), the boundary conditions are specified along straight boundaries in the transformed plane. Also, the coordinate line spacing in the transformed plane is uniform. At this point it should be noted that the actual values of ξ and η are irrelevant. The only quantities required by the finite difference

expressions are the values of $\Delta\xi$ and $\Delta\eta$ which are taken to be unity by construction since cancellation occurs upon substitution into the finite difference expressions.

The generating system of equations, Equations (2.3a) and (2.3b), is solved in the transformed plane. All derivatives are approximated by second-order central finite difference expressions. The resulting set of nonlinear simultaneous difference equations is solved using a point SOR iteration.

Due to the instability in the Navier-Stokes solution near the trailing edge reported by Steger and Bailey [9] and Thompson [10] for O-type coordinate systems, the coordinate systems used in this study were generated using a different outer boundary configuration than shown in Figure 1. All coordinate systems used in this study possessed a "C-shaped" outer boundary as shown in Figure 2. The use of this configuration eliminates the problem of the coordinate lines having to "bend" around the sharp trailing edge.

Consider the two-dimensional doubly-connected region shown in Figure 2. Once again the body is represented by the closed contour Γ_1. However, the "C-shaped" outer boundary is represented by three contours, Γ_3 and the downstream boundaries Γ_2 and Γ_4. The cut in the physical plane is made along the contours Γ_5 and Γ_6. For this configuration, $\eta = \eta_1$ on the contours Γ_5, Γ_1 and Γ_6 and $\eta = \eta_2$ on the contour Γ_3. ξ varies monotonically from $\xi = \xi_1$ on Γ_2 to $\xi = \xi_2$ on Γ_4. Once again the contour Γ_1 in the physical plane maps to the contour Γ_1^* in the transformed plane, Γ_2 maps to Γ_2^*, etc. Since the value of η is constant along the contours Γ_5, Γ_1 and Γ_6, these contours must represent a line

of constant η in the transformed plane. Also, the cut made in the physical plane along the contours Γ_5 and Γ_6 is represented by the re-entrant segments Γ_5^* and Γ_6^* in the transformed plane.

Several different forms of the attraction functions, $P(\xi,\eta)$ and $Q(\xi,\eta)$ from Equations (2.3a) and (2.3b), are given by References [1], [3], [4], and [7]. In this study only η-line contraction was used, so $P(\xi,\eta)$ is taken to be zero. Initially the form of the attraction function, $Q(\xi,\eta)$, was taken to be the form given in the appendix of Reference [2]. The form of $Q(\xi,\eta)$ which gave the best results, however, is presented in the appendix of Reference [4] and Reference [7]. This technique is developed in detail in Appendix B.

III. THE NAVIER-STOKES EQUATIONS IN PRIMITIVE VARIABLES

The time-averaged Navier-Stokes equations for two-dimensional incompressible flow coupled with an algebraic eddy viscosity turbulence model are presented as an alternative to the full Navier-Stokes equations for two-dimensional incompressible turbulent flow. The primitive variable formulation is employed. The resultant equations are non-dimensionalized and transformed to the transformed (ξ,η) plane. The boundary conditions and their application are also presented.

A. The Basic Equations

As stated previously, the full Navier-Stokes equations for incompressible turbulent flow must be solved to accurately predict a high Reynolds number incompressible flowfield. Since an extension to multiple bodies and eventually three-dimensional flow is desired, only the primitive variable formulation will be considered. The full Navier-Stokes equations for two-dimensional incompressible flow are given in the primitive variable formulation by

$$\rho(u_t + uu_x + vu_y) = - p_x + \mu(u_{xx} + u_{yy}) \tag{3.1a}$$

$$\rho(v_t + uv_x + vv_y) = - p_y + \mu(v_{xx} + v_{yy}) \tag{3.1b}$$

$$D = u_x + v_y = 0 \tag{3.1c}$$

where u and v are the velocity components parallel to the x and y directions respectively, p is the pressure, ρ is the fluid density, μ is the molecular viscosity coefficient, and the subscripts x, y, and t represent partial differentiation in the usual manner. Equations (3.1)

theoretically include the turbulent motion of the fluid if the time step size and the spacing of the discrete mesh points are taken to be arbitrarily small. This approach is impractical due to the excessive computational requirements. Some approximate method must be used to model the effects of turbulence.

The time-averaged Navier-Stokes equations for incompressible flow, given in the primitive variables by

$$\rho(\bar{u}_t + \bar{u}\bar{u}_x + \bar{v}\bar{u}_y) = -\bar{p}_x + \mu(\bar{u}_{xx} + \bar{u}_{yy}) - \rho(\overline{u'v'})_y - \rho(\overline{u'^2})_x \qquad (3.2a)$$

$$\rho(\bar{v}_t + \bar{u}\bar{v}_x + \bar{v}\bar{v}_y) = -\bar{p}_y + \mu(\bar{v}_{xx} + \bar{v}_{yy}) - \rho(\overline{u'v'})_x - \rho(\overline{v'^2})_y \qquad (3.2b)$$

$$\bar{D} = \bar{u}_x + \bar{v}_y = 0 \qquad (3.2c)$$

where the over bars indicate time-averaged quantities and the primes indicate fluctuating quantities, were considered in this study. This form was chosen because of the availability of techniques which model the Reynolds stresses, $-\rho(\overline{u'v'})$, $-\rho(\overline{u'^2})$, and $-\rho(\overline{v'^2})$.

The major problem associated with the primitive variable formulation of the Navier-Stokes equations, Equations (3.1), is the lack of a time derivative for pressure. There is no direct way of advancing pressure to the next time level. In fact, the role of pressure in incompressible flow is to somehow adjust itself so that continuity will be satisfied. A Poisson equation in pressure can be obtained by taking the divergence of the momentum equations, Equations (3.1a) and (3.1b). Several forms of this equation are given by Hodge [5] and Shanks [6]. The form used in this study is given by

$$-(p_{xx} + p_{yy}) = (u_x)^2 + 2v_x u_y + (v_y)^2 + D_t \qquad (3.3)$$

where D_t is the time derivative of the continuity equation. Analytically, D is always zero, so D_t will always be zero. Numerically, this is generally not true. The term D_t is retained in Equation (3.3) as a corrective term to adjust the pressure in an attempt to drive continuity to zero.

B. The Turbulence Model

The technique used in this study to model the Reynolds stresses is a slightly modified version of the two-layer algebraic eddy viscosity turbulence model developed by Baldwin and Lomax [2]. In this model, the effects of turbulence are represented by an eddy viscosity coefficient μ_t. That is, the Reynolds stress terms of Equations (3.2a) and (3.2b) are dropped and the molecular viscosity coefficient μ is replaced by $\mu + \mu_t$. Equations (3.2) then become

$$\rho(\bar{u}_t + \bar{u}\bar{u}_x + \bar{v}\bar{u}_y) = -\bar{p}_x + \mu(1 + \epsilon)(\bar{u}_{xx} + \bar{u}_{yy}) \tag{3.4a}$$

$$\rho(\bar{v}_t + \bar{u}\bar{v}_x + \bar{v}\bar{v}_y) = -\bar{p}_y + \mu(1 + \epsilon)(\bar{v}_{xx} + \bar{v}_{yy}) \tag{3.4b}$$

$$D = \bar{u}_x + \bar{v}_y = 0 \tag{3.4c}$$

where ϵ is the ratio of μ_t to μ. In addition, the distribution of vorticity is used to determine the length scale so that finding the edge of the boundary layer is not necessary.

Spatial derivatives of the eddy viscosity have been neglected in both the momentum equations and in the Poisson equation for the pressure. This approximation was applied in order to avoid considerable complication of these equations, but justification was not established.

The method used to model transition is given by Cebeci and Bradshaw [11]. The calculation of the eddy viscosity coefficient is modified by an intermittency factor that accounts for the transitional region that exists between laminar and turbulent regions of a flow. This avoids the assumption that the laminar flow becomes turbulent at the transition point which can in general lead to substantial error. For simplicity of calculation, the body is assumed to be a flat plate. A transition point is calculated on the upper and lower surfaces by assuming that transition occurs at the first minimum pressure point on each surface.

C. The Non-Dimensional Equations in the Transformed Plane

Equations (3.4) and Equation (3.3) can be simplified considerably by using the following non-dimensional variables:

$$x^* \equiv x/L, \qquad y^* \equiv y/L,$$

$$u^* \equiv \bar{u}/U_\infty, \qquad v^* \equiv \bar{v}/U_\infty,$$

$$p^* \equiv (\bar{p} - p_\infty)/\rho U^2_\infty, \qquad t^* \equiv tU_\infty/L,$$

$$Re \equiv \rho U_\infty L/\mu$$

where U_∞ is the freestream velocity, L is the characteristic length, p_∞ is the freestream pressure, and Re is the Reynolds number. After substitution of the non-dimensional variables, with the asterisks dropped for convenience henceforth, Equations (3.4) and Equation (3.3) become

$$u_t + uu_x + vu_y = -p_x + (u_{xx} + u_{yy})(1 + \varepsilon)/Re \tag{3.5a}$$

$$v_t + uv_x + vv_y = -p_y + (v_{xx} + v_{yy})(1 + \varepsilon)/Re \tag{3.5b}$$

$$D = u_x + v_y = 0 \tag{3.5c}$$

$$-(p_{xx} + p_{yy}) = (u_x)^2 + 2v_x u_y + (v_y)^2 + D_t. \tag{3.5d}$$

This set of equations represents the form used for the bulk of this study.

Equations (3.5) must now be transformed into the transformed plane using the relations and definitions given in Appendix A. The resulting transformed equations are given by

$$u_t + u(y_\eta u_\xi - y_\xi u_\eta)/J + v(x_\xi u_\eta - x_\eta u_\xi)/J =$$

$$- (y_\eta p_\xi - y_\xi p_\eta)/J + [(\alpha u_{\xi\xi} - 2\beta u_{\xi\eta} + \gamma u_{\eta\eta})/J^2$$

$$+ (\sigma/J^2)u_\eta + (\tau/J^2)u_\xi]\ (1 + \varepsilon)/Re \tag{3.6a}$$

$$v_t + u(y_\eta v_\xi - y_\xi v_\eta)/J + v(x_\xi v_\eta - x_\eta v_\xi)/J =$$

$$- (x_\xi p_\eta - x_\eta p_\xi)/J + [(\alpha v_{\xi\xi} - 2\beta v_{\xi\eta} + \gamma v_{\eta\eta})/J^2$$

$$+ (\sigma/J^2)v_\eta + (\tau/J^2)v_\xi]\ (1 + \varepsilon)/Re \tag{3.6b}$$

$$D = (y_\eta u_\xi - y_\xi u_\eta + x_\xi v_\eta - x_\eta v_\xi)/J = 0 \tag{3.6c}$$

$$-[(\alpha p_{\xi\xi} - 2\beta p_{\xi\eta} + \gamma p_{\eta\eta})/J^2 + (\sigma/J^2)p_\eta + (\tau/J^2)p_\xi]$$

$$= [(y_\eta u_\xi - y_\xi u_\eta)^2 + 2(y_\eta v_\xi - y_\xi v_\eta)(x_\xi u_\eta - x_\eta u_\xi)$$

$$+ (x_\xi v_\eta - x_\eta v_\xi)^2]/J^2 + D_t \tag{3.6d}$$

Equations (3.6) are now given on a rectangular field with a square grid in the transformed plane. The numerical procedures used to obtain solutions to Equations (3.6) are given in Chapter 4.

D. The Boundary Conditions

The boundary conditions on the surface of the body are given by

$$u = 0 \tag{3.7a}$$

$$v = 0 \tag{3.7b}$$

which are the no-slip boundary conditions for a viscous fluid on the surface of a stationary body with no transpiration. However, the pressure on the wall p_w is unknown and must be calculated. Hodge [5] presents two methods for obtaining the pressure on the body surface.

A Chorin-type pressure iteration utilizing the continuity equation to obtain the wall pressure is given by

$$p_w^{(s+1)} = p_w^{(s)} - \Omega D \tag{3.8a}$$

where s is the iteration counter and Ω is an appropriate acceleration parameter given by Hodge [5] to be

$$\Omega = \omega J^2/[2\Delta t(\alpha+\gamma)] \tag{3.8b}$$

where ω is an acceleration parameter and Δt is the time step size.

Another method of obtaining the wall pressure is to evaluate the normal derivative of the pressure at the wall from the momentum equation. The pressure normal to an η-wall is given by

$$p_n^{(\eta)} = \underset{\sim}{n}^{(\eta)} \cdot \nabla p = (\gamma p_\eta - \beta p_\xi)/J\sqrt{\gamma} \tag{3.9}$$

where $\underset{\sim}{n}^{(\eta)} \cdot \nabla p$ is found from Equation (A.27) in Appendix A. The normal component of the momentum equation for a body with no transpiration and the no-slip boundary condition is given by

$$p_n^{(\eta)} = [\beta p_\xi + y_\xi R\dot{X} - x_\xi R\dot{Y}]/\gamma \tag{3.10a}$$

where

$$RX \equiv -[(-2\beta u_{\xi\eta} + \gamma u_{\eta\eta})/J + (\sigma/J)u_{\eta}]/Re \qquad (3.10b)$$

$$RY \equiv -[(-2\beta v_{\xi\eta} + \gamma v_{\eta\eta})/J + (\sigma/J)v_{\eta}]/Re \qquad (3.10c)$$

The wall pressure can be calculated from Equations (3.10) using one-sided difference equations.

The pressure at a sharp trailing edge is calculated by applying Equations (3.8) or Equations (3.10) to the upper and lower surfaces of the body at the trailing edge. Since these two values are not generally equal, an average is taken to obtain the pressure at the trailing edge.

The freestream boundary conditions are applied at all points on the outer boundary. The freestream conditions are given in terms of the non-dimensional variables by

$$u = \cos \phi \qquad (3.11a)$$

$$v = \sin \phi \qquad (3.11b)$$

$$p = 0 \qquad (3.11c)$$

where ϕ is the angle of attack. The freestream boundary conditions can be applied on the downstream boundary because of the large distance from the trailing edge to the downstream boundary used in this study.

IV. IMPLEMENTATION OF THE NUMERICAL SOLUTION

The transformed equations must now be approximated by finite difference expressions. An outline of the techniques used to develop a finite difference approximation is presented. The general forms of the finite difference expressions used in the approximation are given in Appendix C. The method of solution of the finite difference approximation is discussed. The finite difference approximation for derivatives across the cut is discussed. Various numerical techniques used to improve the stability of the numerical solution are discussed.

A. The Finite Difference Approximation

The transformed Navier-Stokes and Poisson pressure equations, Equations (3.6), must now be represented by a finite difference approximation on the discrete mesh system. Since this finite difference approximation represents a system of nonlinear partial differential equations which are elliptic in space and parabolic in time, the finite difference approximation chosen must accurately reflect these characteristics. Also, consideration must be given to the stability requirements of the method used.

For these reasons, an implicit algorithm was developed which utilized backward-time and central-space differencing techniques. Both first-and second-order differences were considered for the time derivatives. Only second-order differences were used for the spatial derivatives. Since central differences cannot be used to represent spatial derivatives in the wall pressure calculation, Equation (3.8a)

or Equation (3.9), second-order forward differences were used to represent the η-derivatives. The general forms of the finite difference expressions used in this algorithm are given in Appendix C.

At this point, it should be noted that derivatives taken across the "cut" in the physical plane must receive special treatment. With reference to Figure 2, a derivative taken across the contours Γ_5 and Γ_6 in the physical plane is taken across the reentrant segments Γ_5^* and Γ_6^* in the transformed plane. Since x and y are equal along these lines, evaluation is necessary along only one of them. As shown in Figure 3, points in the transformed (ξ,η) plane which are located at (I1-N,1) and (I2+N,1) for $N \leq I1$ have the same coordinates in the physical (x,y) plane. With this in mind, the finite difference expressions given in Appendix C can be used to obtain

$$(f_\eta)_{I1-N,1} = (f_\eta)_{I2+N,1} = (f_{I1-N,2} - f_{I2+N,2})/2 \tag{4.1a}$$

$$(f_{\eta\eta})_{I1-N,1} = (f_{\eta\eta})_{I2+N,1} = f_{I1-N,2} - 2f_{I1-N,1} + f_{I1+N,2} \tag{4.1b}$$

$$(f_{\xi\eta})_{I1-N,1} = (f_{\xi\eta})_{I2+N,1}$$

$$= (f_{I1-N-1,2} - f_{I1-N+1,2} + f_{I2+N+1,2}$$

$$-f_{I2+N-1,2})/4 \tag{4.1c}$$

where f is an arbitrary function of ξ and η. This insures that the derivatives taken across the reentrant segments are continuous.

The nonlinear system of algebraic equations which is formed by the application of the appropriate finite difference expressions from Appendix C to Equations (3.6) is solved using a point SOR iteration.

The calculation of a linearly optimum acceleration parameter for an iteration of this type follows the procedure given by Thompson [7].

B. Numerical Stabilizing Techniques

Several purely numerical techniques were implemented in an attempt to obtain a stable solution. These techniques are needed because of the nonphysical oscillations of the dependent variables which can develop in regions of steep gradients. These oscillations, or numerical instabilities, can cause an otherwise stable solution to become unstable and diverge.

There are two possible approaches which can be taken to enhance the stability of a numerical solution. One possible approach is to treat the symptoms of the numerical instability by filtering or equivalently, adding an artificial viscosity. The other approach is to attempt to alleviate the cause of the instability.

A basic filter considered in this study is the switched form of the Shuman filter given by Harten and Zwas [12]. The two-dimensional Shuman filter for a general function f is given by

$$f_{i,j} = f_{i,j} + \frac{\theta}{8}\left[f_{i+1,j} + f_{i-1,j} + f_{i,j+1} + f_{i,j-1} - 4f_{i,j}\right] \quad (4.2)$$

where $\theta = 1$ for the simple Shuman filter. Since this technique has the effect of adding an artificial viscosity, the effective Reynolds number will be lowered considerably if the Shuman filter is applied at all points in the field. However, this will eliminate all of the oscillations. The characteristics of this filter can be improved if it is locally applied only when a certain waveform is encountered.

If an N-waveform is to be filtered, θ would be set to unity if an N-waveform is encountered but would be set to zero otherwise. Thus, only the two sharp points of the N-waveform would be filtered. Similar statements can be made in relation to a filter for W-waveforms or a W-filter. Only the central point of a W-waveform is filtered. It should be noted that the N-filter, and especially the W-filter, add no diffusion at all to most of the field. The purpose of the N-filter and the W-filter is not to eliminate the oscillations, but to control them so the solution does not diverge.

The filter is applied after each time step. It could be applied after each iteration but this often causes convergence difficulties. In addition, the technique of filtering can be applied repetitively after each time step to further reduce the amplitude of the oscillation.

Another technique which introduces an artificial viscosity is a fourth-order smoother related to that used by Baldwin and MacCormack [13]. Several forms of this smoother were implemented. The form which was finally considered simply replaces $(1+\varepsilon)$ in Equations (3.6) with $(1+\varepsilon+\nabla^2 pJ\Delta tRe)$, where $\nabla^2 p$ is the Laplacian of the pressure and Δt is the time step size. This technique introduces a significant artificial viscosity only in regions where the Laplacian of the pressure is large.

Most of the attempts to alleviate the cause of the instability center around the representation of the convective derivatives. The form given by Equations (3.1) is the non-conservative form. The term $uu_x + vu_y$ in Equation (3.1a) is actually the expanded form of $(u^2)_x + (uv)_y$ after cancellation of the continuity equation, Equation (3.1c), with $D = 0$. Analytically these two terms are

equivalent, numerically they may not be. Four different techniques were tested and are outlined here. Only terms in the x-momentum equations are shown since extension to the y-momentum equation is similar.

Two possible representations of the convective derivatives are noted in MacCormack [14]. The convective derivative $(u^2)_x$ can be represented as the average of a product (AOP) given by

$$(u^2)_x = \frac{1}{2}\left[(u^2)_{i+1} - (u^2)_{i-1}\right] . \tag{4.3}$$

Equation (4.3) can itself cause instabilities as explained in Reference [14]. A more stable technique is the representation of the convective derivative $(u^2)_x$ as the product of an average (POA). This form is given by

$$(u^2)_x = \frac{1}{4}\left[(u_{i+1} + u_i)^2 - (u_i + u_{i-1})^2\right] . \tag{4.4}$$

These techniques are described in greater detail by Reference [14].

An attempt to improve the stability of the techniques given by Equation (4.3) and Equation (4.4) was made by including a mass residual correction. This technique replaces $uu_x + vu_y$ in Equation (3.1a) with

$$(u^2)_x + (uv)_y - u(u_x + v_y) \tag{4.5}$$

which is analytically equivalent to the non-conservative form. The terms $(u^2)_x$ and $(uv)_y$ can be replaced by terms of the form of Equation (4.3) or Equation (4.4).

Beam and Warming [15] used a technique to linearize the convective terms to prevent the instability. The form used in this study is

given by

$$(u^2)^{n+1} = (u^2)^n + 2u^n(u^{n+1} - u^n) \tag{4.6}$$

where n is the time step number. Equation (4.6) is a second-order Taylor series expansion for $(u^2)^{n+1}$ about $(u^2)^n$. Since u^n is known, this representation for $(u^2)^{n+1}$ is linear.

V. RESULTS

The computer code used in this study was written by Joe F. Thompson as part of the current research of the Department of Aerospace Engineering at Mississippi State University for the NASA Langley Research Center. The test case considered in this study was the flow-field generated by an NACA 64A010 airfoil section at an angle of attack of two degrees and a Reynolds number of 2,000,000.

All the coordinate systems considered in this study were generated using the method of Chapter 2. The ξ-attraction function $P(\xi,\eta)$ was obtained by the simultaneous solution of Equations (2.3) after the initial guess had been obtained. The initial guess was formed by placing the η-line distribution produced by the contraction near the body on each ξ-line. Now the ξ-attraction function is given by the product of $P(\xi,\eta)$ as obtained above and a decaying exponential based on $-0.2d$ where d is the distance from the body. The η-attraction function $Q(\xi,\eta)$ was varied to obtain different η-line distributions near the airfoil. In all cases, the coordinate system was "C-shaped" with 113 ξ-lines and 51 η-lines in the field. There were 72 unique points on the airfoil. The downstream and outer boundaries were located 10 chord lengths from the airfoil. In addition, a Neumann boundary condition was imposed on the η-lines at the downstream boundary. A typical coordinate system generated during this study is shown in Figure 4. The region of the field near the airfoil is shown in Figure 5. The convergence criteria used for all coordinate systems was 10^{-6}.

Similarly, the following techniques were common to most of the Navier-Stokes solutions attempted during this study.

(1) A linear start in 100 steps was used with a time step size of 0.01.

(2) The first time step was run using first-order time differencing with no turbulence.

(3) The basic turbulence model without the transition point calculation outlined in Chapter 3 was initiated along with second-order time differencing after the first time step.

(4) The non-conservative forms of the momentum equations, Equations (3.6a) and (3.6b), were considered without the stabilizing techniques described in Chapter 4.

(5) A zero first time derivative projection for the initial guess at the next time level was used.

(6) The pressure on the boundary was obtained from Equations (3.8) with $\omega = 0.5$.

(7) The field pressure acceleration parameter was 1.0. The velocities were multiplied by 2.0 in the calculation of an optimum acceleration parameter.

(8) The velocity and pressure convergence criteria were 10^{-5} and 10^{-4} respectively.

(9) Partial convergence was accepted after 100 iterations.

(10) All computations were performed on a UNIVAC 1100 series computer.

Exceptions to these procedures are noted in the course of the discussion of results which follows.

The first type of coordinate system considered in this study was generated by forming a composite function for $Q(\xi,\eta)$ as described by Thompson [7]. A Blasius boundary layer profile was joined to a quartic polynomial at the second line inside the boundary layer. The first coordinate system generated using this technique (CS1) had 10 η-lines contracted into the boundary. The η-line distributions in the boundary layer for CS1 at the point of maximum thickness of the airfoil and the leading edge of the airfoil are shown in Figures 6.a and 6.b respectively.

CS1 was used to generate a solution which diverged at $t = 1.05$. The divergence occurred near the leading edge at approximately the first η-line off the body. As shown in Figure 7, a pressure peak also occurred near this point. It was thought that the divergence was caused by an insufficient number of η-lines being contracted into the boundary layer.

To remedy this problem, a second coordinate system (CS2) was generated using the same technique which had 20 η-lines contracted into the boundary layer. CS2 was used extensively to test the various numerical techniques implemented during this study. The η-line distributions for CS2 are shown in Figures 8.a and 8.b. As shown in Figure 8.b, the η-lines are contracted much closer to the airfoil at the leading edge than previously shown in Figure 6.b .

CS2 was used to generate a solution which diverged at $t = 1.08$. The divergence occurred in the region of the leading edge at the eighth η-line off the body. Once again, a pressure peak occurred in the region near the divergence as shown in Figure 9. This solution was restarted from $t = 1.00$ using the W-filter as described in Chapter 4.

Once again, the iteration diverged at t = 1.08 and the pressure behavior was the same. Repeating this procedure using the N-filter described in Chapter 4 also had little effect on the divergence of the iteration or the pressure behavior. Also, the repetitive application of the W-filter after each time step had little effect on the behavior of the solution. The solution was again restarted from t = 1.00 but with a new initial guess for each time step. The initial guess at the new time step was given by the previous time step solution. This also had little effect on the divergence or the pressure behavior. Applying the W-filter from t = 0.00 also had no significant effect. Applying the simple Shuman filter, Equation (4.2), with $\theta = 1$, to the restart of this solution produced a more rapid divergence.

An attempt was then made using CS2 to generate a solution using the momentum equation, Equations (3.10), to obtain the pressure on the boundary. The iteration diverged at t = 1.08 and exhibited the same behavior as before. The pressures on the airfoil obtained using the momentum equation were essentially the same as those obtained using the continuity equation. Restarting the solution from t = 1.00 and using the N-filter had little effect on the divergence of the pressure behavior. Once again, taking the initial guess at the new time step to be the previous time step solution had no significant effect.

Since each of these attempts was diverging soon after the start up procedure was completed, several different start-up procedures were tested using CS2 as the coordinate system. A 100 step cosine start was implemented. The iteration diverged at t = 0.86. The cosine start

was no longer considered since it diverged before the linear start. Another start-up procedure tested was the use of first-order backward time differences for the time derivatives. This also proved unsuccessful, as the iteration diverged at t = 0.94. This was sooner than the divergence of the second-order backward time differencing previously used. In addition, a 100 step linear start was used with the velocity multiple being 1.0 instead of 2.0 in the optimum acceleration parameter calculation. This had a destabilizing effect on the iteration. Instabilities appeared in the solution as early as t = 0.80. Divergence occurred at t = 0.98. The pressure behavior was essentially the same as stated previously.

Several attempts were made to stabilize the solution by representing the convective terms as described in Chapter 4 using CS2 as the coordinate system. The product of the average representation of the convective terms (POA), given by Equation (4.4), was implemented in an attempt to stabilize the solution. This iteration diverged at t = 0.74. Convergence was lost as early as t = 0.50. Once again, the pressure behavior was similar to that shown in Figure 9. The mass residual correction, given by Equation (4.5), was used in conjunction with the POA representation of the convective terms in an attempt to stabilize the iteration. The combination of these techniques proved to be unsuccessful since this iteration diverged sooner than the iteration without the mass residual correction. The average of the product representation of the convective terms (AOP), given by Equation (4.3), was implemented in conjunction with the mass residual correction,

given by Equation (4.5), in an attempt to stabilize the solution. This was also unsuccessful, as the iteration diverged at t = 0.54. The AOP representation was not considered without the mass residual correction because of the nonlinear instability reported by MacCormack [14].

In addition, a second-order linearization of the form given by Equation (4.6) was implemented to enhance the stability of the solution. This was unsuccessful in that the divergence of the iteration occurred at t = 0.53. The divergence of the iteration once again occurred in the same region.

Since the iteration was diverging in the same region of the field for all cases using the coordinate system CS2, a coordinate system was generated (CS3) with 20 η-lines contracted into the boundary layer using the attraction function given by Roberts [16]. This attraction function is a continuous exponential function. This eliminates any problems associated with discontinuities in the derivatives of the η-line distribution which result from a composite function being chosen for the attraction function. Figures 10.a and 10.b show the distribution of η-lines in the boundary layer at the point of maximum thickness and the leading edge of the airfoil respectively.

CS3 was used to generate a solution which did not diverge and seemed to be converging at time t = 2.00. However, this solution was worthless as shown in Figure 11. This invalid pressure distribution was obtained from an equally invalid velocity field. This behavior was caused by the looseness of the coordinate system convergence criteria. The distance at the leading edge to the first η-line off the

body was 2×10^{-6}, which is the same order of magnitude as the convergence criteria. This problem could be alleviated by generating a coordinate system with a decreased convergence criteria or by decreasing the number of η-lines contracted into the boundary layer.

The latter approach was implemented and a coordinate system (CS4) was generated with 10 η-lines contracted into the boundary layer. The distance at the leading edge to the first η-line off the body was 2.6×10^{-4}. The distributions of the η-lines in the boundary layer at the point of maximum thickness and leading edge of the airfoil are shown in Figures 12.a and 12.b respectively.

CS4 was used to generate a solution which diverged at $t = 1.18$. This solution was more well-behaved than the solution obtained using CS3. The pressure distribution obtained at $t = 1.00$ is shown in Figure 13. Once again, a pressure peak occurred in the region where the divergence originated. Application of the W-filter to the restart of this solution had no significant effect.

A new coordinate system was generated (CS5) which utilized the techniques outlined in Appendix B. The distributions of the η-lines in the boundary layer at the point of maximum thickness and the leading edge of the airfoil are shown in Figures 14.a and 14.b respectively. As an attempt to reduce the roundoff error, σ and τ are calculated directly from $P(\xi,\eta)$ and $Q(\xi,\eta)$. This iteration diverged at $t = 1.08$ and exhibited the same behavior as observed for CS3. The MacCormack fourth-order smoother as described in Chapter 4 was implemented in an attempt to stabilize the solution. This iteration

had not diverged at t = 2.00, but convergence was lost as early as t = 1.90. The maximum iteration error occurred near the upper surface trailing edge at the sixteenth η-line off the body. The pressure distribution obtained at t = 1.90 is shown in Figure 15. The poor representation of the flowfield was caused by the turbulence model inaccurately representing the eddy viscosity. The eddy viscosity coefficient obtained from the turbulence model was so large that the flow separated at the leading edge on both the upper and lower surfaces. This separation was caused by the assumption that the entire flowfield was turbulent. However, the flow near the leading edge was actually laminar. This led to the inclusion of the transition point calculation as discussed in Chapter 3.

At this point in time, adequate computational facilities became unavailable locally. This necessitated a conversion of all programs for compatibility with the CDC computational facilities available at NASA Langley Research Center. Because of this delay, only preliminary data is available from the new techniques implemented during the conversion.

CS5 was regenerated with a convergence criteria of 10^{-8}. Using this new coordinate system, a solution was generated by including the transition point calculation outlined in Chapter 3, in addition to the fourth-order MacCormack smoother and the calculation of σ and τ from $P(\xi,\eta)$ and $Q(\xi,\eta)$. Preliminary results indicate that the transition point on the lower surface is calculated to be near the trailing edge of the airfoil. Previously, all of the lower surface was turbulent. Now all of the lower surface is laminar. This trend occurred from

t = 0.00 to t = 0.70, the last time level where data is available. Also, full convergence has been obtained up to this time level.

VI. CONCLUSIONS

The development of the boundary-fitted coordinate systems have made the numerical solution of the Navier-Stokes equations for high Reynolds number incompressible turbulent flow feasible. Several numerical techniques were implemented and evaluated during this study. The following list summarizes the most important results of this evaluation.

(1) The non-conservative formulation of the Navier-Stokes equations gives better results than formulations involving AOP or POA representations of the convective terms. In addition, the mass residual correction and the second-order linearization were also ineffective.

(2) The MacCormack smoother was the only filter which enhanced the stability of the solution significantly. The Shuman filter, N-filter, and W-filter did not significantly affect the stability of the solution. The ineffectiveness of these filters can be attributed to the larger time step size of implicit methods. The filter was not applied as often over the same time interval as it would have been for the explicit methods for which it was developed.

(3) The pressure on the boundary can be obtained from the continuity equation via a Chorin-type iteration or from the component of the momentum equation normal to the boundary. However, using the continuity equation seems to improve the stability of the solution slightly.

(4) Preliminary data indicates that the addition of an intermittency factor at the transition point significantly improves the effects of the algebraic turbulence model used in this study.

(5) Better results are obtained for coordinate systems which have a continuous distribution of coordinate lines with small convergence criteria (10^{-8}).

The preliminary results of the final solution described in Chapter 5 are the most encouraging to date. This solution should be continued in an attempt to obtain a valid steady-state solution.

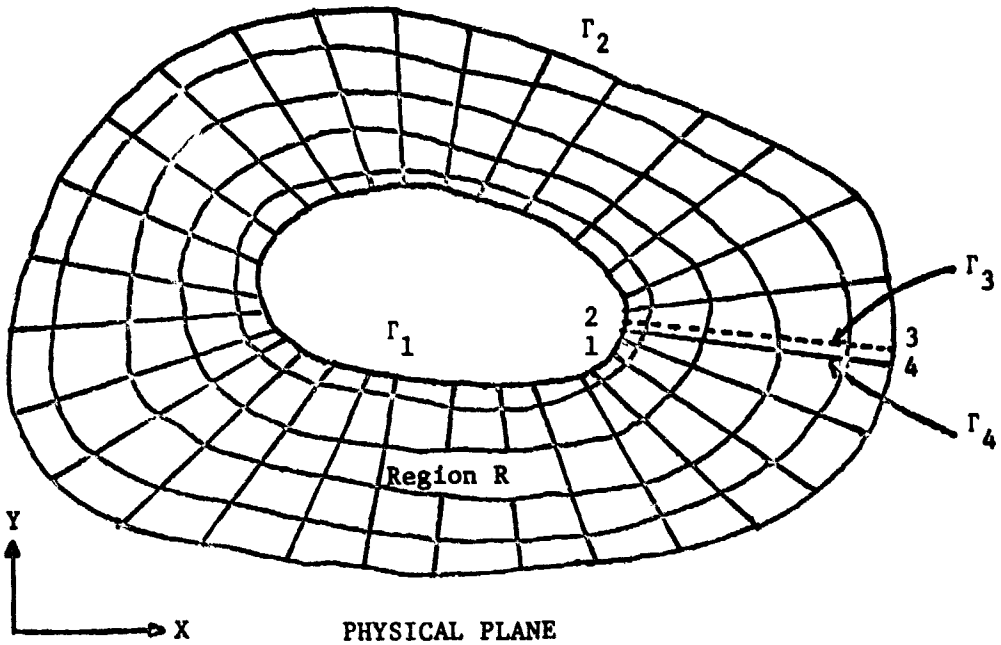

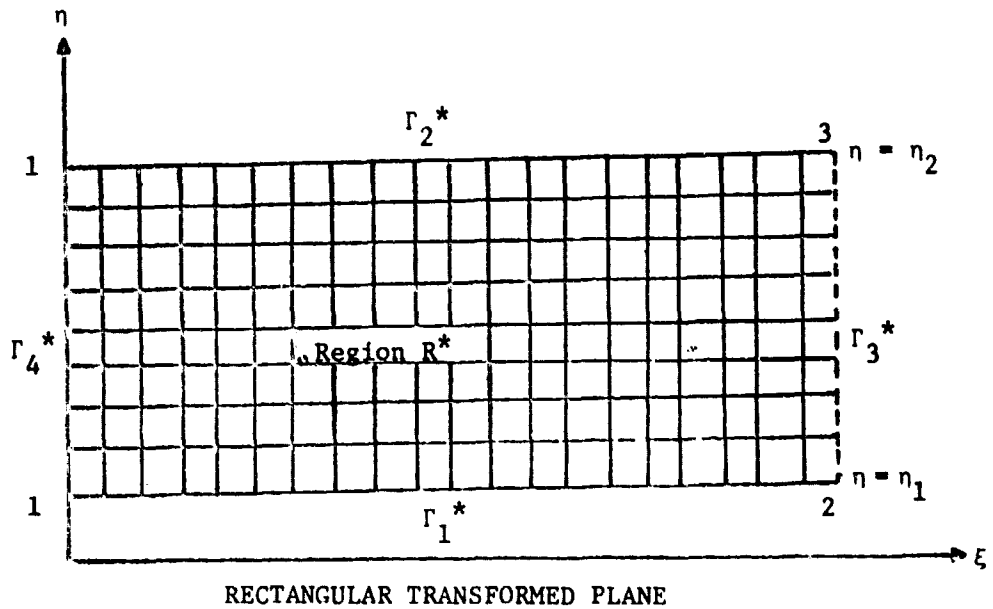

Figure 1. Coordinate Transformation - O-Type Outer Boundary

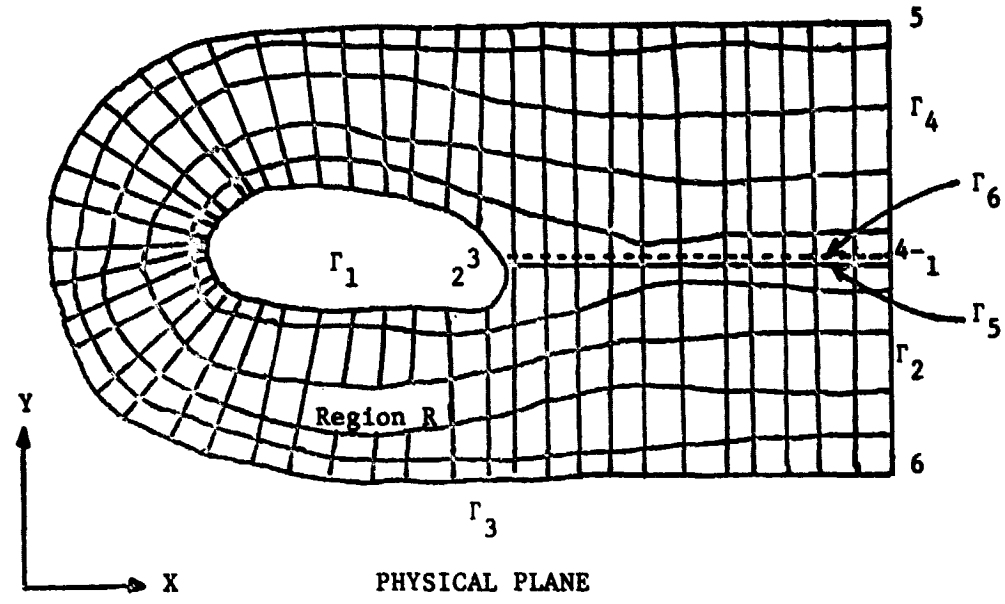

PHYSICAL PLANE

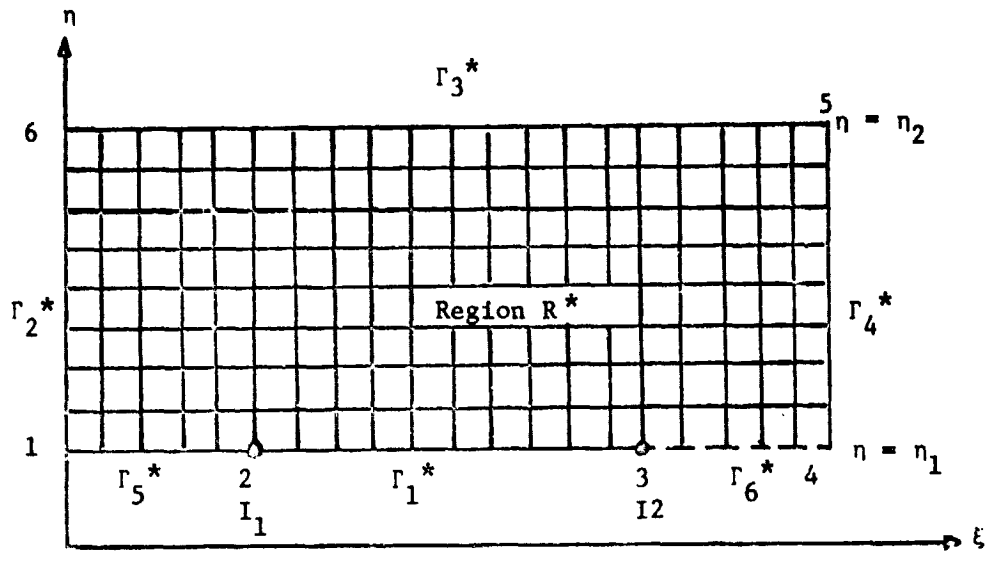

RECTANGULAR TRANSFORMED PLANE

Figure 2. Coordinate Transformation - C-Type Outer Boundary

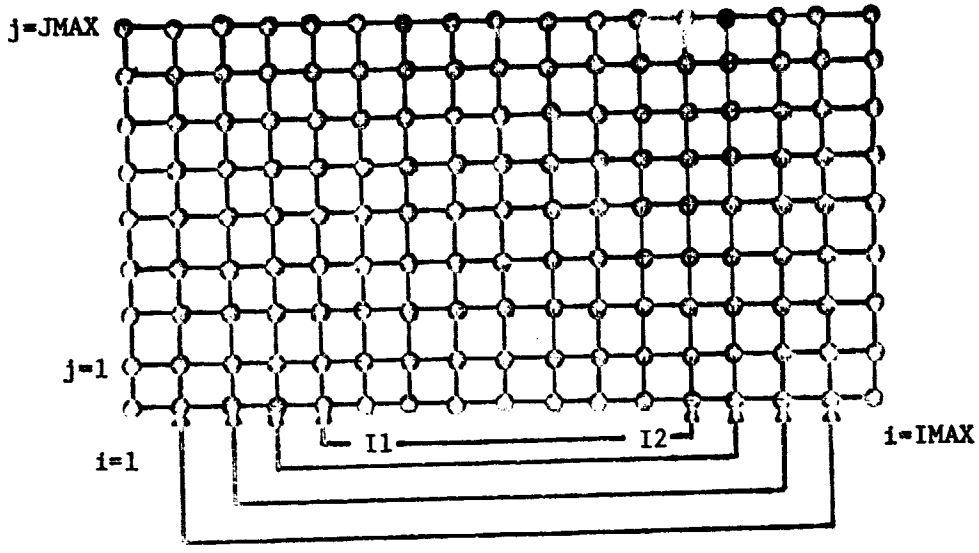

Figure 3. Computational Grid

Figure 4. Typical Coordinate System-NACA 64A010

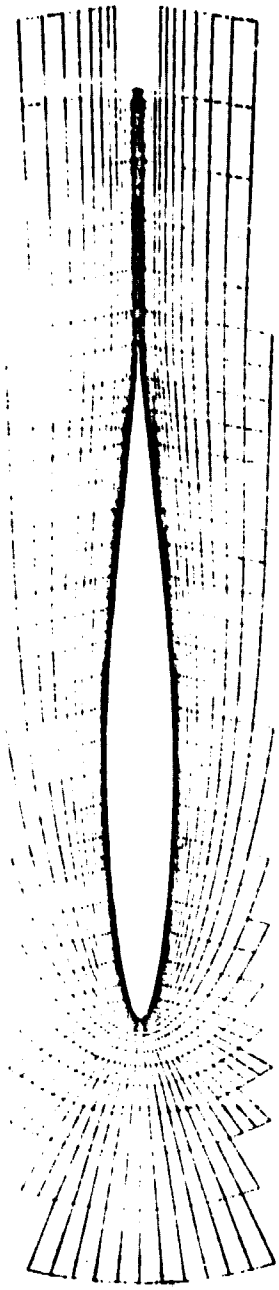

Figure 5. Region of Field Near Body - NACA 64A010

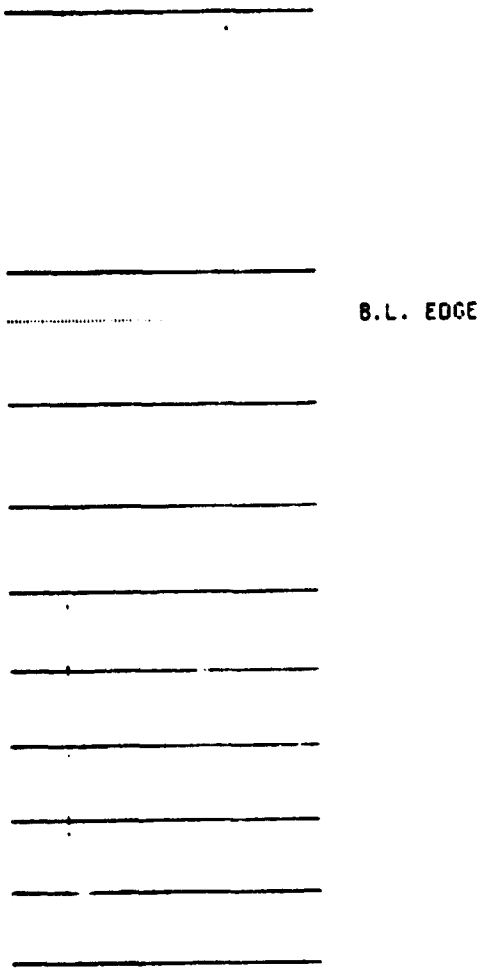

Figure 6a. Eta-Line Distribution at Point of Maximum Airfoil Thickness - CS2

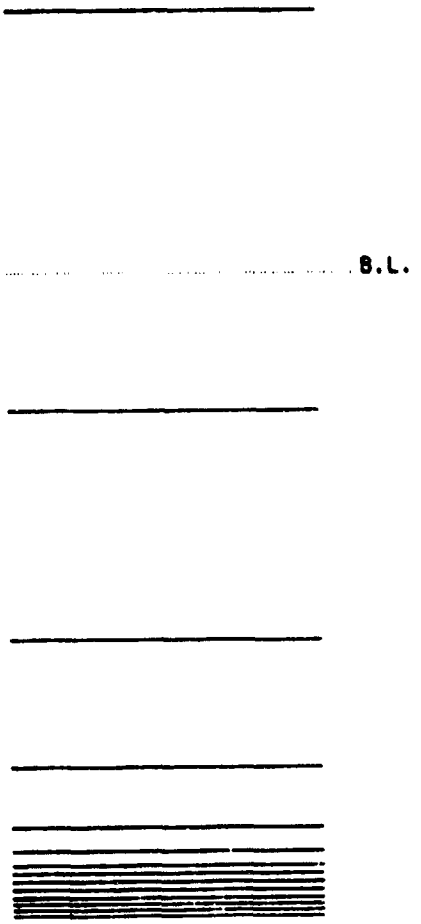

Figure 6b. Eta-Line Distribution at Leading Edge - CS1

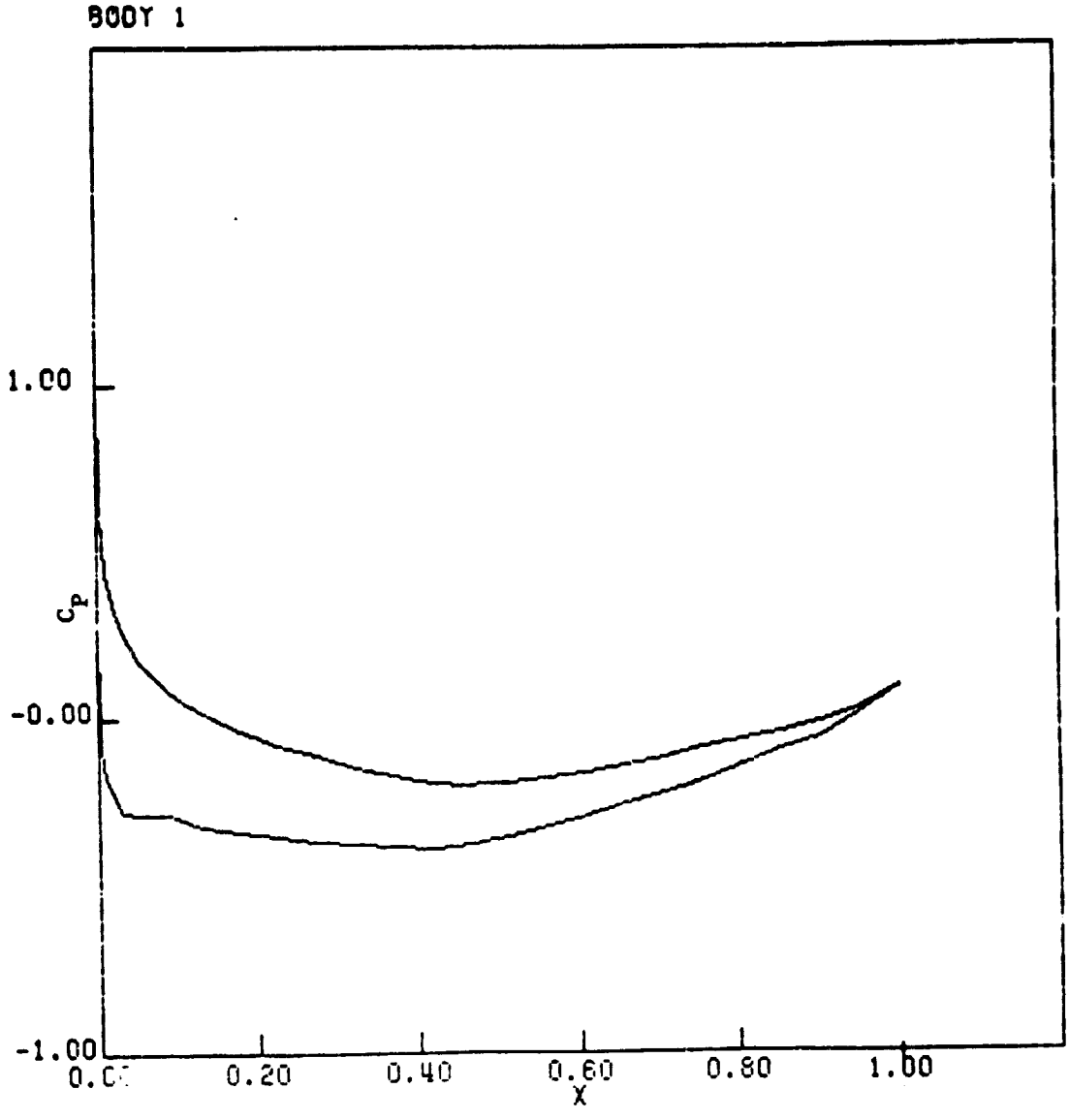

Figure 7. Pressure Distribution - CS1 - t = 1.04

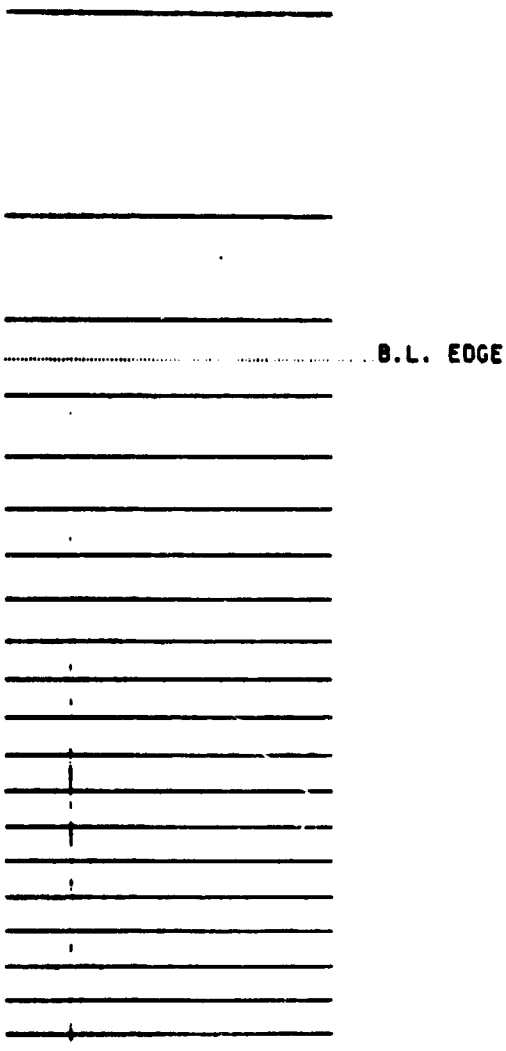

B.L. AT YMAX

Figure 8a. Eta-Line Distribution at Point of Maximum Airfoil Thickness - CS2

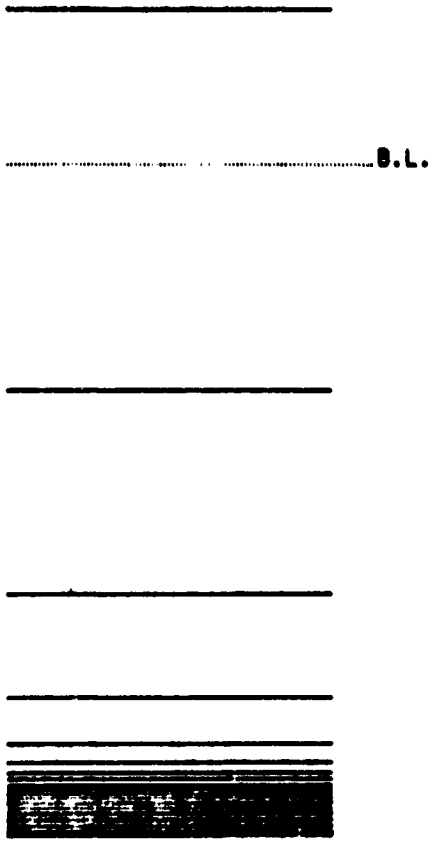

B.L. AT XMIN

Figure 8b. Eta-Line Distribution at Leading Edge - CS2

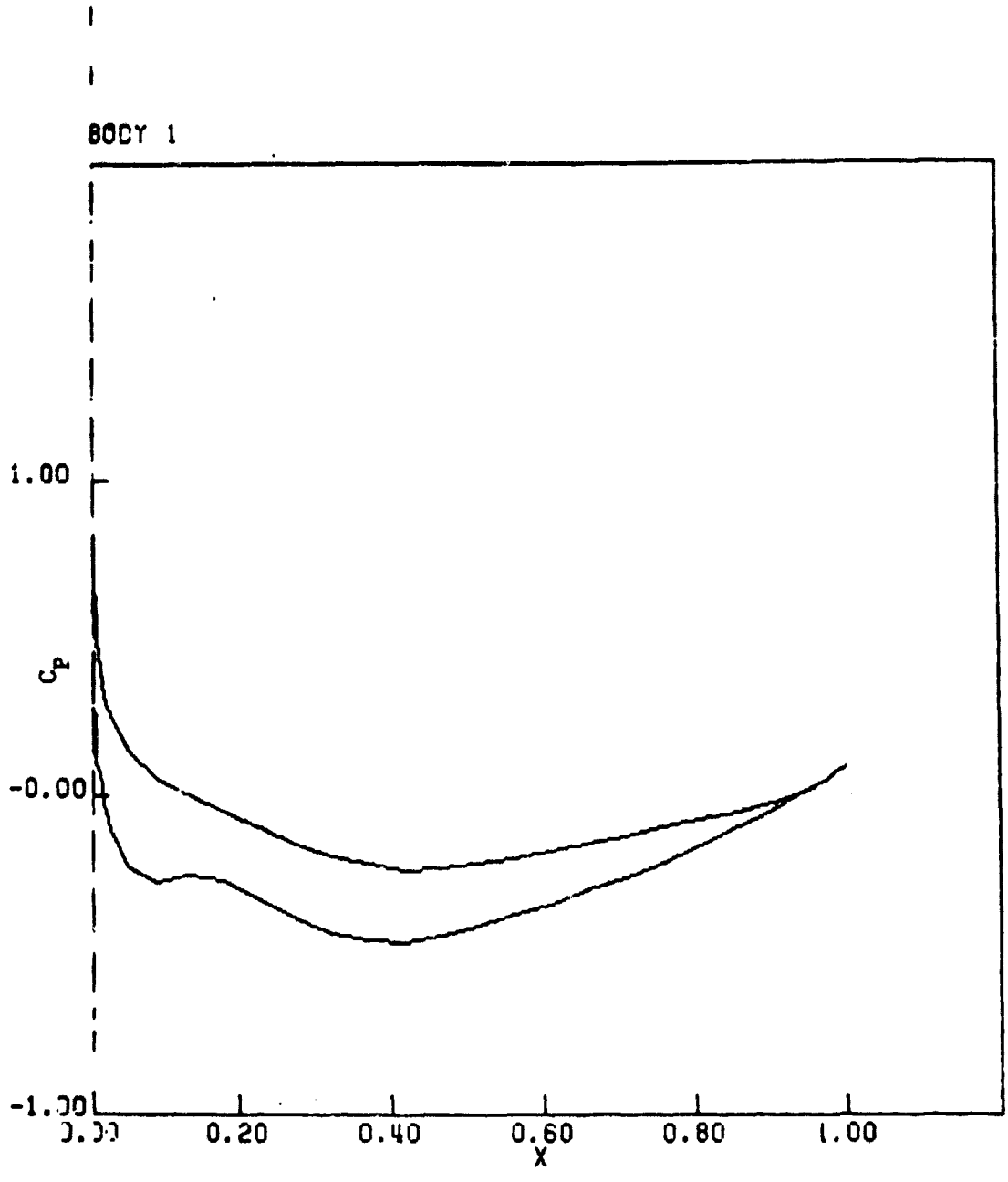

Figure 9. Pressure Distribution - CS2 - t = 1.00

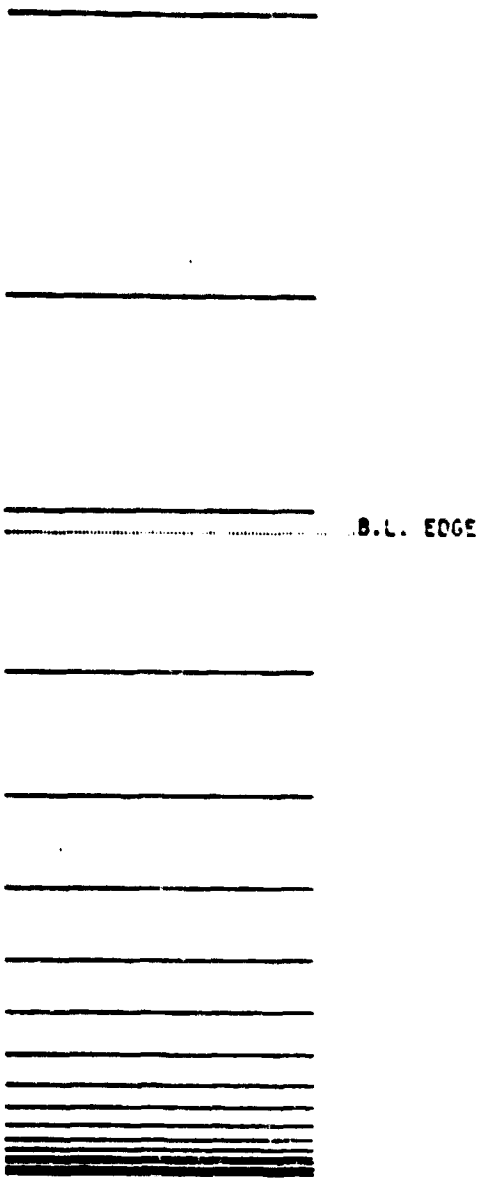

Figure 10a. Eta-Line Distribution at Point of Maximum Airfoil Thickness - CS3

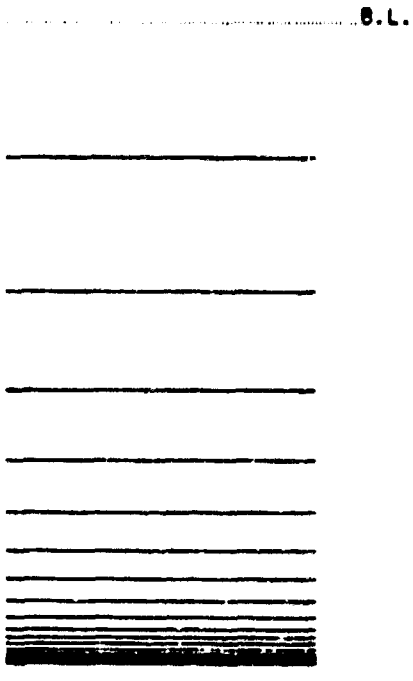

Figure 10b. Eta-Line Distribution at Leading Edge - CS3

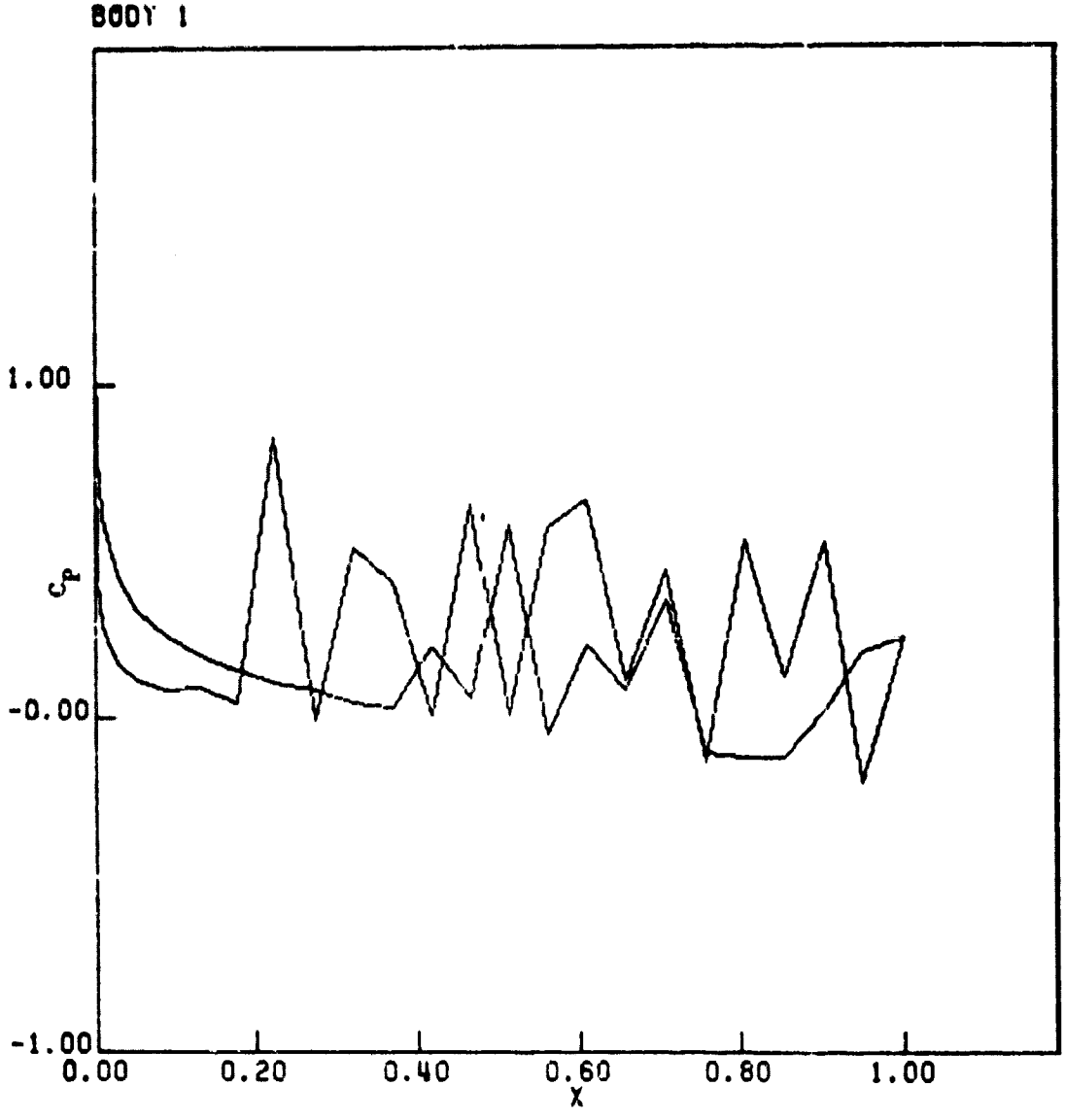

Figure 11. Pressure Distribution - CS3 - t = 2.00

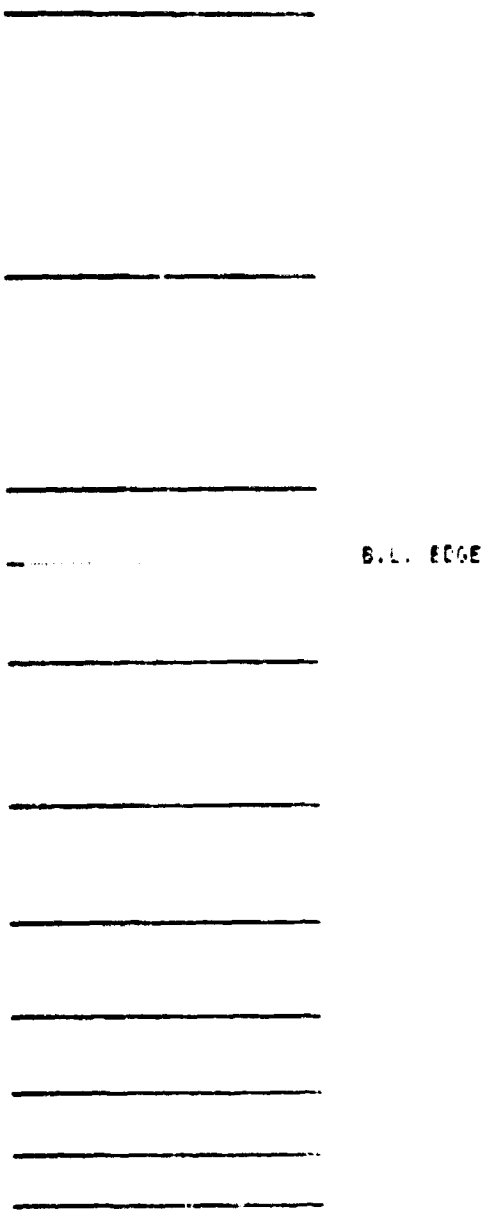

Figure 12a. Eta-Line Distribution at Point of Maximum Airfoil Thickness - CS4

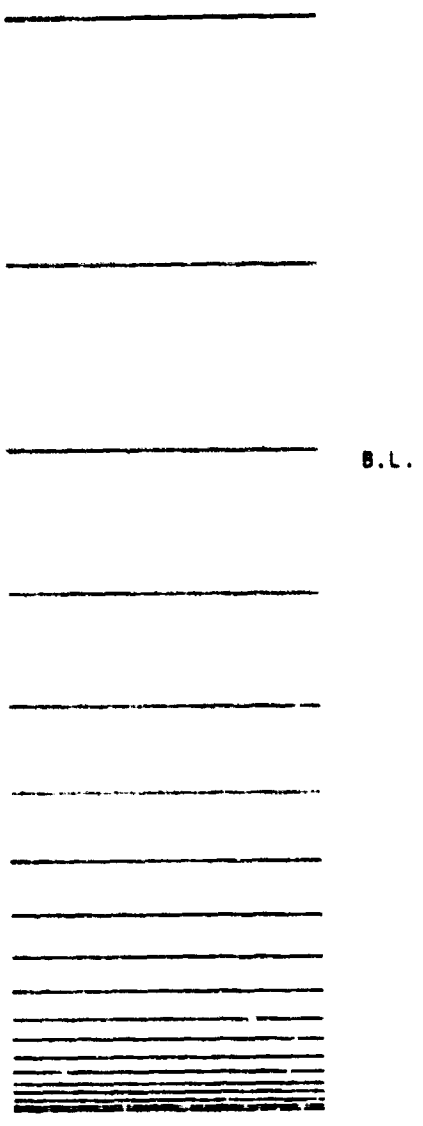

Figure 12b. Eta-Line Distribution at Leading Edge - CS4

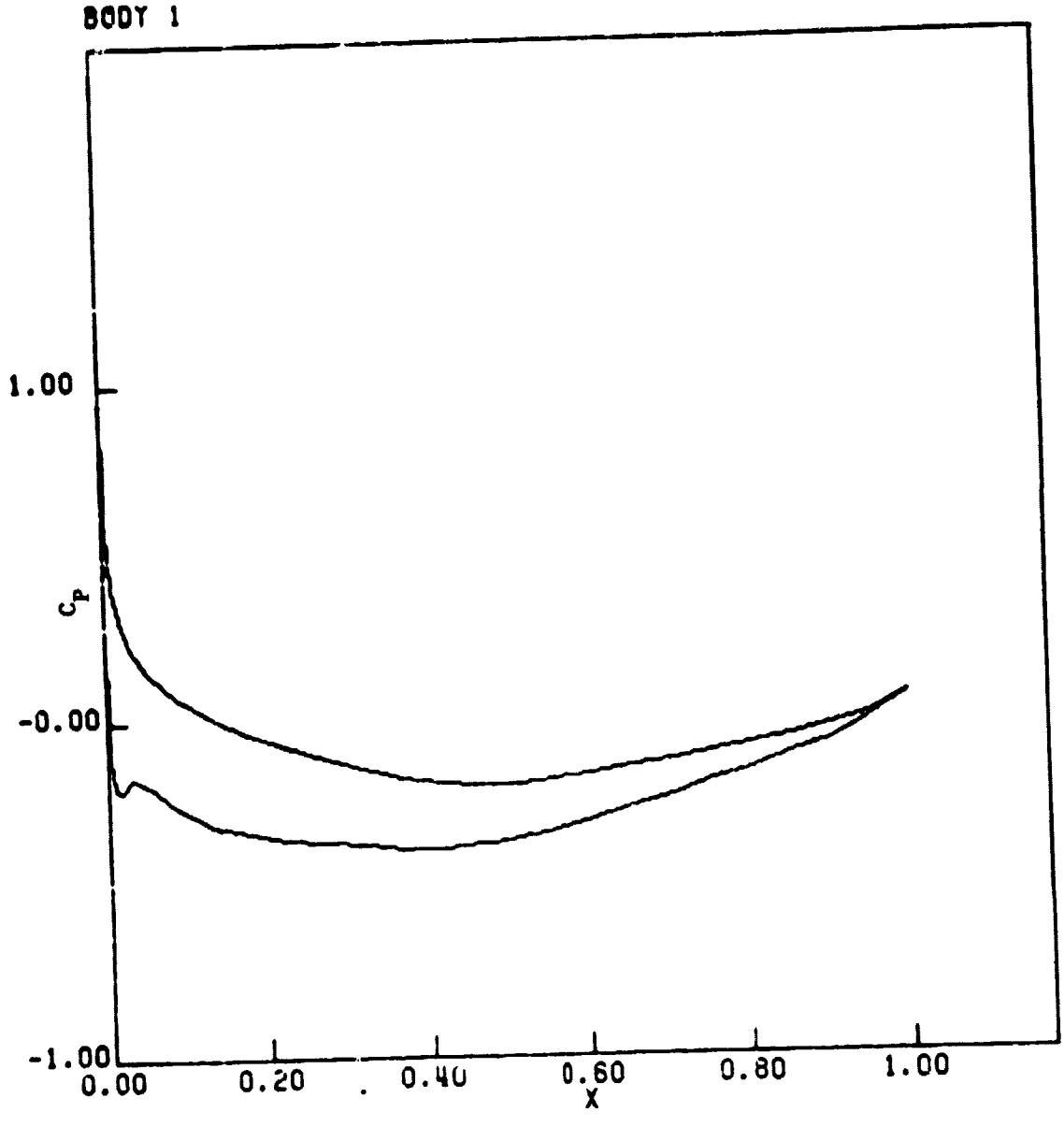

Figure 13. Pressure Distribution - CS4 -- t = 1.00

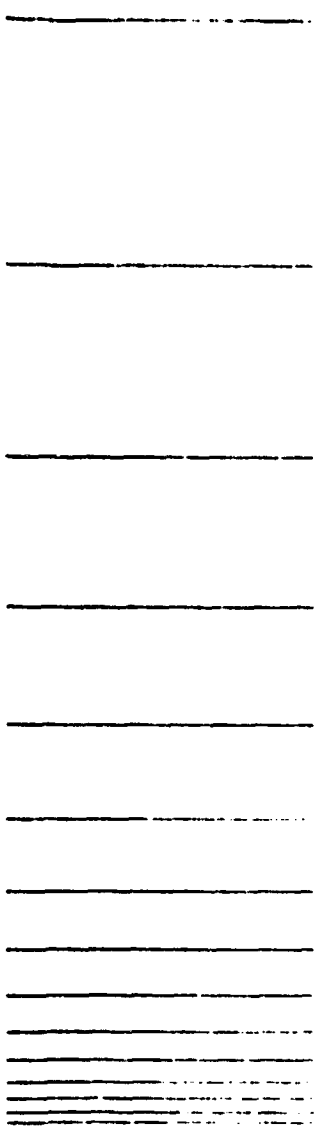

Figure 14a. Eta-Line Distribution at Point of Maximum Airfoil Thickness - CS5

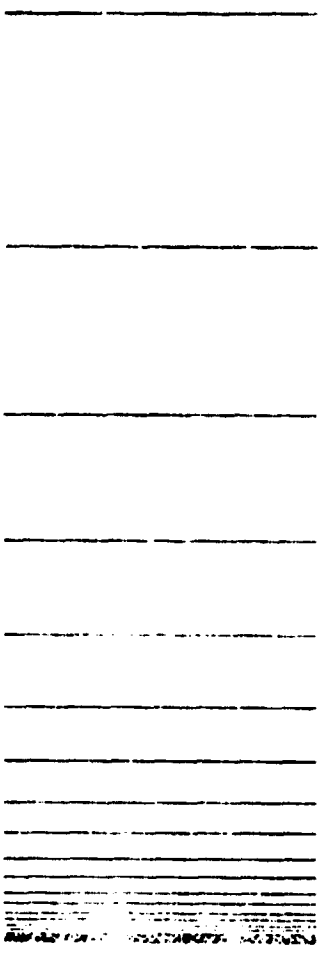

Figure 14b. Eta-Line Distribution at Leading Edge - CS5

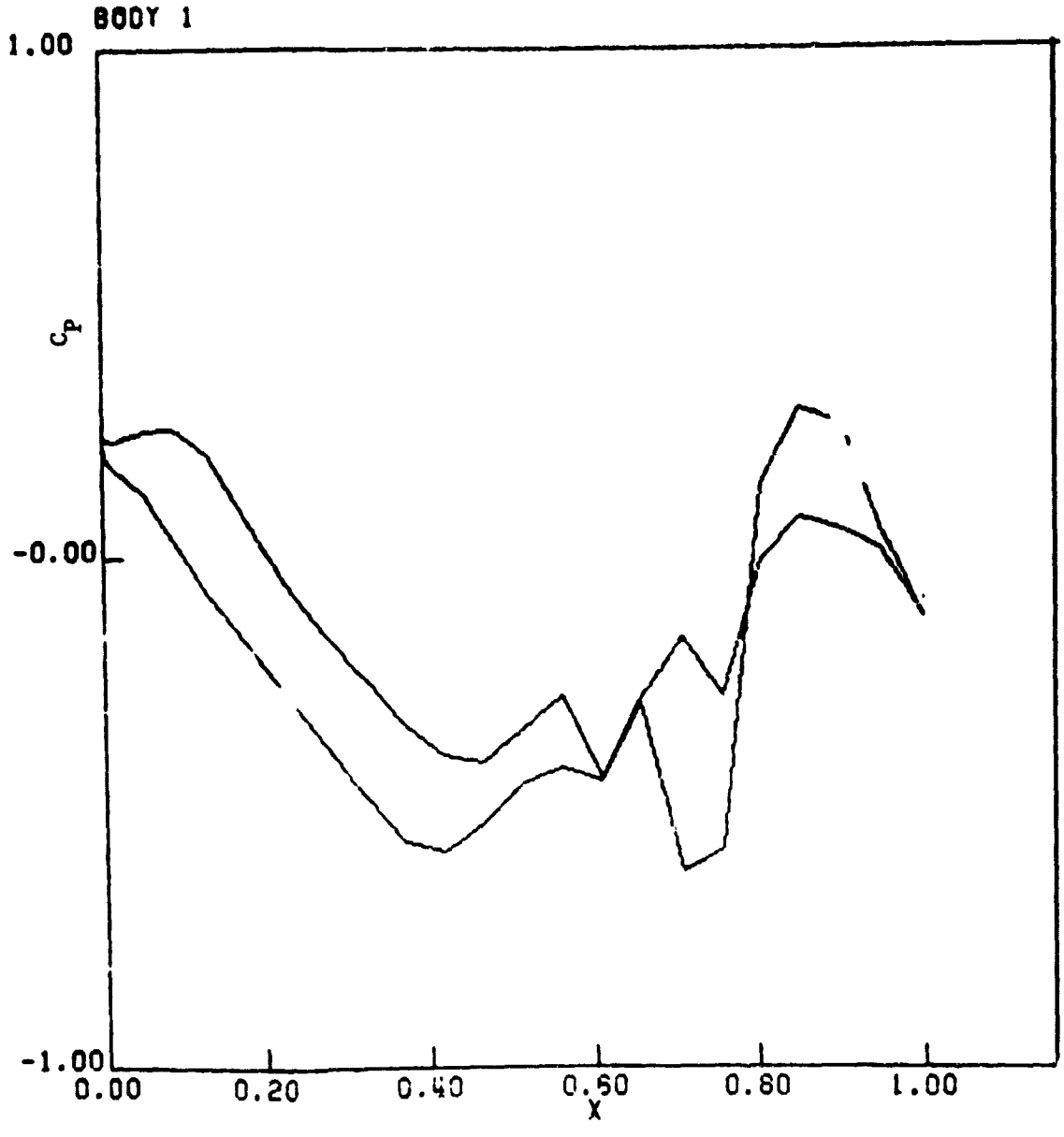

Figure 15. Pressure Distribution - CS5 - t = 1.90

APPENDIX A

Various Relations in the Transformed Plane

This Appendix contains many of the pertinent definitions and relations in the transformed (ξ,η) plane. Thompson, Thames, and Mastin [1] present a comprehensive set of relations and the notation used in Reference [1] is retained here. Similarly, the following function definitions are applicable:

$f(x,y,t)$ - A twice continuously differentiable scalar function of x,y and t

$F(x,y) = \underset{\sim}{i}\, F_1(x,y) + \underset{\sim}{j}\, F_2(x,y)$ - A continuously differentiable vector-valued function; $\underset{\sim}{i}$ and $\underset{\sim}{j}$ are the conventional Cartesian coordinate unit vectors.

It should be noted that all derivative transformations given here are in the geometrically non-conservative form.

Definitions of the Transformation

$$\alpha \equiv x_\eta^2 + y_\eta^2 \tag{A.1}$$

$$\beta \equiv x_\xi x_\eta + y_\xi y_\eta \tag{A.2}$$

$$\gamma \equiv x_\xi^2 + y_\xi^2 \tag{A.3}$$

$$Dx \equiv \alpha x_{\xi\xi} - 2\beta x_{\xi\eta} + \gamma x_{\eta\eta} \tag{A.4}$$

$$Dy \equiv \alpha y_{\xi\xi} - 2\beta y_{\xi\eta} + \gamma y_{\eta\eta} \tag{A.5}$$

$$\sigma \equiv (y_\xi Dx - x_\xi Dy)/J \tag{A.6}$$

$$\tau \equiv (x_\eta Dy - y_\eta Dx)/J \tag{A.7}$$

$$J \equiv x_\xi y_\eta - x_\eta y_\xi \tag{A.8}$$

Where J is the determinant of the Jacobian matrix.

Derivative Transformations

$$f_x = (\partial f/\partial x)_{y,t} = (y_\eta f_\xi - y_\xi f_\eta)/J \qquad (A.9)$$

$$f_y = (\partial f/\partial y)_{x,t} = (x_\xi f_\eta - x_\eta f_\xi)/J \qquad (A.10)$$

$$\begin{aligned} f_{xx} = (\partial^2 f/\partial x^2)_{y,t} = {} & (y_\eta^2 f_{\xi\xi} - 2y_\xi y_\eta f_{\xi\eta} + y_\xi^2 f_{\eta\eta})/J^2 \\ & + (y_\eta^2 y_{\xi\xi} - 2y_\xi y_\eta y_{\xi\eta} + y_\xi^2 y_{\eta\eta})(x_\eta f_\xi - x_\xi f_\eta)/J^3 \\ & + (y_\eta^2 x_{\xi\xi} - 2y_\xi y_\eta x_{\xi\eta} + y_\xi^2 x_{\eta\eta}) \\ & (y_\xi f_\eta - y_\eta f_\xi)/J^3 \end{aligned} \qquad (A.11)$$

$$\begin{aligned} f_{yy} = (\partial^2 f/\partial y^2)_{x,t} = {} & (x_\eta^2 f_{\xi\xi} - 2x_\xi x_\eta f_{\xi\eta} + x_\xi^2 f_{\eta\eta})/J^2 \\ & + (x_\eta^2 y_{\xi\xi} - 2x_\xi x_\eta y_{\xi\eta} + x_\xi^2 y_{\eta\eta})(x_\eta f_\xi - x_\xi f_\eta)/J^3 \\ & + (x_\eta^2 x_{\xi\xi} - 2x_\xi x_\eta x_{\xi\eta} + x_\xi^2 x_{\eta\eta}) \\ & (y_\xi f_\eta - y_\eta f_\xi)/J^3 \end{aligned} \qquad (A.12)$$

$$\begin{aligned} f_{xy} = {} & [(x_\xi y_\eta + x_\eta y_\xi)\, f_{\xi\eta} - x_\xi y_\xi f_{\eta\eta} - x_\eta y_\eta f_{\xi\xi}]/J^2 \\ & + [x_\eta y_\eta x_{\xi\xi} - (x_\xi y_\eta + x_\eta y_\xi)\, x_{\xi\eta} + x_\xi y_\xi x_{\eta\eta}](y_\eta f_\xi - y_\xi f_\eta)/J^3 \\ & + [x_\eta y_\eta y_{\xi\xi} - (x_\xi y_\eta + x_\eta y_\xi)\, y_{\xi\eta} + x_\xi y_\xi y_{\eta\eta}] \\ & (x_\xi f_\eta - x_\eta f_\xi)/J^3 \end{aligned} \qquad (A.13)$$

Vector Derivative Transformations

Laplacian:

$$\begin{aligned} \nabla^2 f = {} & (\alpha f_{\xi\xi} - 2\beta f_{\xi\eta} + \gamma f_{\eta\eta})/J^2 + [(\alpha x_{\xi\xi} - 2\beta x_{\xi\eta} + \gamma x_{\eta\eta})(y_\xi f_\eta - y_\eta f_\xi) \\ & + (\alpha y_{\xi\xi} - 2\beta y_{\xi\eta} + \gamma y_{\eta\eta})(x_\eta f_\xi - x_\xi f_\eta)]/J^3 \end{aligned} \qquad (A.14)$$

or

$$\nabla^2 f = (\alpha f_{\xi\xi} - 2\beta f_{\xi\eta} + \gamma f_{\eta\eta} + \sigma f_{\eta} + \tau f_{\xi})/J^2 \qquad \text{(A.15)}$$

Gradient:

$$\underset{\sim}{\nabla} f = [(y_{\eta} f_{\xi} - y_{\xi} f_{\eta})\,\underset{\sim}{i} + (x_{\xi} f_{\eta} - x_{\eta} f_{\xi})\underset{\sim}{j}]/J \qquad \text{(A.16)}$$

Divergence:

$$\underset{\sim}{\nabla} \cdot \underset{\sim}{F} = [y_{\eta}(F_1)_{\xi} - y_{\xi}(F_1)_{\eta} + x_{\xi}(F_2)_{\eta} - x_{\eta}(F_2)_{\xi}]/J \qquad \text{(A.17)}$$

Curl:

$$\underset{\sim}{\nabla} \times \underset{\sim}{F} = \underset{\sim}{k}[y_{\eta}(F_2)_{\xi} - y_{\xi}(F_2)_{\eta} - x_{\xi}(F_1)_{\eta} + x_{\eta}(F_1)_{\xi}]/J \qquad \text{(A.18)}$$

Unit Tangent and Normal Vectors

Normal to η-Line:

$$\underset{\sim}{n}^{(\eta)} \equiv \underset{\sim}{\nabla}\eta/|\underset{\sim}{\nabla}\eta| = (-y_{\xi}\underset{\sim}{i} + x_{\xi}\underset{\sim}{j})/\sqrt{\gamma} \qquad \text{(A.19)}$$

Normal to ξ-Line:

$$\underset{\sim}{n}^{(\xi)} \equiv \underset{\sim}{\nabla}\xi/|\underset{\sim}{\nabla}\xi| = (y_{\eta}\underset{\sim}{i} - x_{\eta}\underset{\sim}{j})/\sqrt{\alpha} \qquad \text{(A.20)}$$

Tangent to η-Line:

$$\underset{\sim}{t}^{(\eta)} \equiv \underset{\sim}{n}^{(\eta)} \times \underset{\sim}{k} = (x_{\xi}\underset{\sim}{i} + y_{\xi}\underset{\sim}{j})/\sqrt{\gamma} \qquad \text{(A.21)}$$

Tangent to ξ-Line:

$$\underset{\sim}{t}^{(\xi)} \equiv \underset{\sim}{n}^{(\xi)} \times \underset{\sim}{k} = -(x_{\eta}\underset{\sim}{i} + y_{\eta}\underset{\sim}{j})/\sqrt{\alpha} \qquad \text{(A.22)}$$

Vector Components Tangent and Normal to ξ and η-Lines

$$F_{\underset{\sim}{n}}^{(\eta)} \equiv \underset{\sim}{n}^{(\eta)} \cdot \underset{\sim}{F} = (-y_{\xi}F_1 + x_{\xi}F_2)/\sqrt{\gamma} \qquad \text{(A.23)}$$

$$F_{\underset{\sim}{t}}^{(\eta)} \equiv \underset{\sim}{t}^{(\eta)} \cdot \underset{\sim}{F} = (x_{\xi}F_1 + y_{\xi}F_2)/\sqrt{\gamma} \qquad \text{(A.24)}$$

$$F_{\underset{\sim}{n}}^{(\xi)} \equiv \underset{\sim}{n}^{(\xi)} \cdot \underset{\sim}{F} = (y_{\eta}F_1 - x_{\eta}F_2)/\sqrt{\alpha} \qquad \text{(A.25)}$$

$$F_{\underset{\sim}{t}}^{(\xi)} \equiv \underset{\sim}{t}^{(\xi)} \cdot \underset{\sim}{F} = -(x_{\eta}F_1 + y_{\eta}F_2)/\sqrt{\alpha} \qquad \text{(A.26)}$$

Directional Derivatives

$$\partial f/\partial \underset{\sim}{n}^{(\eta)} \equiv \underset{\sim}{n}^{(\eta)} \cdot \underset{\sim}{\nabla} f = (\gamma f_{\eta} - \beta f_{\xi})/J\sqrt{\gamma} \tag{A.27}$$

$$\partial f/\partial \underset{\sim}{t}^{(\eta)} \equiv \underset{\sim}{t}^{(\eta)} \cdot \underset{\sim}{\nabla} f = f_{\xi}/\sqrt{\gamma} \tag{A.28}$$

$$\partial f/\partial \underset{\sim}{n}^{(\xi)} \equiv \underset{\sim}{n}^{(\xi)} \cdot \underset{\sim}{\nabla} f = (\alpha f_{\xi} - \beta f_{\eta})/J\sqrt{\alpha} \tag{A.29}$$

$$\partial f/\partial \underset{\sim}{t}^{(\xi)} \equiv \underset{\sim}{t}^{(\xi)} \cdot \underset{\sim}{\nabla} f = - f_{\eta}/\sqrt{\alpha} \tag{A.30}$$

APPENDIX B

Concentration of Coordinate Lines Near a Body

Consider the coordinate system generation Equations (2.3) applied to concentric circular boundaries of radius r_1 and r_2. With $\eta = 1$ on the inner boundary, $\eta = J$ on the outer boundary, and ξ varying monotonically from 1 to ξ_2 around these boundaries, the solution of Equations (2.3) can be given in the form

$$x = r(\eta) \cos \left[2\pi \left(\frac{\xi-1}{\xi_2-1}\right)\right] \tag{B.1a}$$

$$y = r(\eta) \sin \left[2\pi \left(\frac{\xi-1}{\xi_2-1}\right)\right] . \tag{B.1b}$$

Substitution of these expressions into either of the equations of (2.3) with $P(\xi,\eta) = 0$ yields

$$\frac{r''}{r'} - \frac{r'}{r} + Q(\xi,\eta) = 0 . \tag{B.2}$$

This can be made a perfect differential by taking the control function $Q(\xi,\eta)$ of the form

$$Q(\xi,\eta) \equiv - \frac{f''(\eta)}{f'(\eta)} \tag{B.3}$$

where the minus sign has been introduced merely for convenience.

Substituting Equation (B.3) into Equation (B.2) yields

$$\frac{r''}{r'} - \frac{r'}{r} - \frac{f''}{f'} = 0 \tag{B.4}$$

which can be integrated twice to yield

$$r(\eta) = c_2 e^{c_1 f(\eta)} . \tag{B.5}$$

The constants of integration may be evaluated from the boundary

conditions, $r(1) = r_1$, $r(J) = r_2$, so that

$$r(\eta) = r_1 \{(r_2/r_1)^{\left[\frac{f(\eta) - f(1)}{f(J) - f(1)}\right]} \quad . \tag{B.6}$$

This equation may then be solved for $f(\eta)$ to yield

$$\frac{f(\eta) - f(1)}{f(J) - f(1)} = \frac{\ln[\frac{r(\eta)}{r_1}]}{\ln[\frac{r_2}{r_1}]} \quad . \tag{B.7}$$

If the distance from the body to the Nth η-line is specified to be r_n, the following equation must be satisfied:

$$\frac{f(N) - f(1)}{f(J) - f(1)} = \frac{\ln[\frac{r_N}{r_1}]}{\ln[\frac{r_2}{r_1}]} \quad . \tag{B.8}$$

It should be noted that the form of $f(\eta)$ is still arbitrary, subject to Equation (B.8). The form* used in this study is given by

$$f(\eta) = \eta K^{\eta-1} \tag{B.9}$$

where K is a constant which must satisfy the nonlinear equation

$$\frac{NK^{N-1} - 1}{JK^{J-1} - 1} = \frac{\ln[\frac{r_N}{r_1}]}{\ln[\frac{r_2}{r_1}]} \quad . \tag{B.10}$$

Once K has been determined from Equation (B.10), the control function $Q(\xi,\eta)$ is determined from Equations (B.3) and (B.9) to be

$$Q(\xi,\eta) = -\frac{(2 + \eta \ln K)}{(1 + \eta \ln K)} \ln K \quad . \tag{B.11}$$

*The form of $f(\eta)$ was obtained from Reference [17].

Although the above analysis was developed for circular boundaries, the effect will generally be the same for arbitrary boundary configurations.

The procedure which gave the best results was to fix the distance of the $\eta = 2$ line at one one-hundredth of the boundary layer thickness from the body. Therefore, $r_N = r(2)$ is given by

$$r_N = \frac{0.05}{\sqrt{Re}} + r_1 \ . \tag{B.12}$$

It should be noted that r_1 was set equal to the radius of a circle circumscribed about the body and that r_2 was set equal to the radius of the circular arc which represents a portion of the outer boundary. Now r_N and N have been specified so K is obtained by solving Equation (B.10) using a false position iteration.

APPENDIX C

General Finite Difference Expressions

This appendix summarizes the finite difference expressions for a general function $f(\xi,\eta,t)$ which are necessary for implementation of the procedures outlined in Chapter IV. It should be noted that since the step size in the transformed plane is unity, it does not appear in the spatial difference expressions. For convenience, two short conventions are used in this appendix. All difference equations apply at the point denoted by the space subscripts (i,j) and the time superscript (n). The subscripts (i,j) and superscript (n) are understood where they are omitted. In this appendix, only time derivatives and ξ-derivatives are shown.

Time Derivative Approximations

First-Order Backwards:

$$f_t^n \approx (-f^{n-1} + f^n)/\Delta t \tag{C.1}$$

Second-Order Backwards:

$$f_t^n \approx (f^{n-2} - 4f^{n-1} + 3f^n)/2\Delta t \tag{C.2}$$

Spatial Derivative Approximations (Second-Order Only)

First Derivative, Central Difference:

$$f_\xi \approx f_{i+1,j} - f_{i-1,j} \tag{C.3}$$

First Derivative, Forward Difference:

$$f_\xi \approx (-f_{i+2,j} + 4f_{i+1,j} - 3f_{i,j})/2 \tag{C.4}$$

First Derivative, Backward Difference:

$$f_{\xi} \approx (f_{i-2,j} - 4f_{i-1,j} + 3f_{i,j})/2 \tag{C.5}$$

Second Derivative, Central Difference:

$$f_{\xi\xi} \approx f_{i+1,j} - 2f_{i,j} + f_{i-1,j} \tag{C.6}$$

Cross Derivative, Central Difference:

$$f_{\xi\eta} \approx (f_{i+1,j+1} - f_{i+1,j-1} - f_{i-1,j+1} + f_{i-1,j-1})/4 \tag{C.7}$$

Cross Derivative, ξ-Forward Difference and η-Central Difference:

$$f_{\xi\eta} \approx (-f_{i+2,j+1} + f_{i+2,j-1} + 4(f_{i+1,j+1} - f_{i+1,j-1}) - 3(f_{i,j+1} - f_{i,j-1}))/4 \tag{C.8}$$

Cross Derivative, ξ-Backward Difference and η-Central Difference:

$$f_{\xi\eta} \approx (f_{i-2,j+1} - f_{i-2,j-1} - 4(f_{i-1,j+1} - f_{i-1,j-1}) - 3(f_{i,j+1} - f_{i,j-1}))/4 \tag{C.9}$$

Cross Derivative, ξ-Central Derivative and η-Forward Difference:

$$f_{\xi\eta} \approx (f_{i-1,j+2} - f_{i+1,j+2} + 4(f_{i+1,j+1} - f_{i-1,j+1}) - 3(f_{i+1,j} - f_{i-1,j}))/4 \tag{C.10}$$

References

1. Thompson, J. F., Thames, F. C., and Mastin, C. W., "Boundary-Fitted Curvilinear Coordinate Systems for Solution of Partial Differential Equations on Fields Containing any Number of Arbitrary Two-Dimensional Bodies", NASA CR-2729 (1976).

2. Baldwin, B. S. and Lomax, H., "Thin Layer Approximation and Algebraic Model for Separated Turbulent Flows", AIAA Paper 78-257, AIAA 16th Aerospace Sciences Meeting (1978).

3. Bearden, J. H., "A High Reynolds Number Numerical Solution of the Navier-Stokes Equations in Stream Function-Vorticity Form", M.S. Thesis, Mississippi State University (1977).

4. Reddy, R. N., "Numerical Solution of Incompressible Navier-Stokes Equations in Integro-Differential Formulation Using Boundary-Fitted Coordinte System, "Ph.D. Dissertation, Mississippi State University (1977).

5. Hodge, J. K., "Numerical Solution of Incompressible Laminar Flow about Arbitrary Bodies in Body-Fitted Curvilinear Coordinates", Ph.D. Disseration, Mississippi State University (1975).

6. Shanks, S. P., "Numerical Simulation of Viscous Flow about Submerged Arbitrary Hydrofoils using Non-Orthogonal, Curvilinear Coordinates", Ph.D. Dissertation, Mississippi State University (1977).

7. Thompson, J. F., "Numerical Solution of Flow Problems using Body-Fitted Coordinate Systems", Lecture Series in Computational Fluid Dynamics, von Karman Inst. for Fluid Dynamics, Belgium (1978).

8. Thames, F. C., "Numerical Solution of the Incompressible Navier-Stokes Equations about Arbitrary Two-Dimensional Bodies", Ph.D. Dissertation, Mississippi State University (1975).

9. Steger, J. L. and Bailey, H. E., "Calculation of Transonic Aileron Buzz", AIAA Paper 79-0134, 17th Aerospace Sciences Meeting (1979).

10. Thompson, D. S., "A Comparison of a Numerically Computed Airfoil Pressure Distribution with Experimental Results", Southeastern Regional Student Paper Conference, AIAA (1979).

11. Cebeci, L. and Bradshaw, P., "Momentum Transfer in Boundary Layers, Hemisphere Publishing Corporation, Washington (1977).

12. Harten, A. and Zwas, G., "Switched Numerical Shuman Filters for Shock Calculations", Journal of Engineering Mathematics, 6,2 (1972).

13. Baldwin, B. S. and MacCormack, R. W., "Interaction of Strong Shock Wave with Turbulent Boundary Layer", AIAA Paper 74-558, Palo Alto, California, June 1974.

14. MacCormack, R. W., Numerical Solution of the Interaction of a Shock Wave with a Laminar Boundary Layer", Lecture Notes in Physics, 8, (1971).

15. Beam, R. M. and Warming, R. F., "An Implicit Factored Scheme for the Compressible Navier-Stokes Equations", AIAA Journal, 16,4 (1978).

16. Roberts, G., "Computational Meshes for Boundary Layer Problems", Lecture Notes in Physics, 8,(1971).

17. Warsi, Z. U. A. and Thompson, J. F., "Machine Solutions of Partial Differential Equations in the Numerically Generated Coordinate Systems", MSSU-EIRS-ASE-77-1, Mississippi State University (1976).